Article

The Mechanism of Borane-Amine Dehydrocoupling with Bifunctional Ruthenium Catalysts

Alexander N Marziale, Anja Friedrich, Isabel Klopsch, Markus Drees, Vinicius R Celinski, Jörn Schmedt auf der Günne, and Sven Schneider

J. Am. Chem. Soc., **Just Accepted Manuscript** • DOI: 10.1021/ja311092c • Publication Date (Web): 09 Aug 2013

The Mechanism of Borane-Amine Dehydrocoupling with Bifunctional Ruthenium Catalysts

Alexander N. Marziale,[‡] Anja Friedrich,[†] Isabel Klopsch,[¶] Markus Drees,[†] Vinicius R. Celinski,[§] Jörn Schmedt auf der Günne,[§] and Sven Schneider[*,†,‡,¶]*

Technische Universität München, Department Chemie, Lichtenbergstr. 4, 85747 Garching b. München, Germany, Ludwig-Maximilians-Universität München, Department Chemie und Biochemie, Butenandtstr. 5-13, 81377 München, Germany, Friedrich-Alexander-Universität Erlangen-Nürnberg, Department Chemie und Pharmazie, Egerlandstr. 1, 91058 Erlangen, Germany, and Georg-August-Universität Göttingen, Tammannstr. 4, 37077 Göttingen, Germany.

sven.schneider@chemie.uni-goettingen.de

RECEIVED DATE

[†] Technische Universität München

[§] Ludwig-Maximilians-Universität

[‡] Friedrich-Alexander-Universität Erlangen-Nürnberg

[¶] Georg-August-Universität Göttingen

ABSTRACT: Borane-amine adducts have received considerable attention, both as vectors for chemical hydrogen storage and as precursors for the synthesis of inorganic materials. Transition metal catalyzed ammonia-borane ($H_3N–BH_3$, AB) dehydrocoupling offers, in principle the possibility of large gravimetric hydrogen release at high rates and the formation of B–N polymers with well-defined microstructure. Several different homogeneous catalysts were reported in the literature. The current mechanistic picture implies that the release of aminoborane (e.g. Ni carbenes and Shvo's catalyst) results in formation of borazine and 2 equiv. H_2 while one equiv. H_2 and polyaminoborane are obtained with catalysts that also couple the dehydroproducts (e.g. Ir and Rh diphosphine and pincer catalysts). However, in comparison with their rapidly growing number, the amount of experimental studies that deal with mechanistic details is still limited. Here, we present a comprehensive experimental and theoretical study about the mechanism of AB dehydrocoupling to polyaminoborane with ruthenium amine/amido catalysts, which exhibit particularly high activity. Based on kinetics, trapping experiments, polymer characterization by ^{11}B MQMAS solid-state NMR, spectroscopic experiments with model substrates, and density functional theory (DFT) calculations, we propose for the amine catalyst $[Ru(H)_2PMe_3\{HN(CH_2CH_2P\textit{t}Bu_2)_2\}]$ two mechanistically connected catalytic cycles that account both for metal mediated substrate dehydrogenation to aminoborane and catalyzed polymer enchainment by formal aminoborane insertion into a $H–NH_2BH_3$ bond. Kinetic results and polymer characterization also indicate that amido catalyst $[Ru(H)PMe_3\{N(CH_2CH_2P\textit{t}Bu_2)_2\}]$ does not undergo the same mechanism as was previously proposed in a theoretical study.

INTRODUCTION

In recent years, borane amine adducts, particularly parent H_3N-BH_3 (AB), attracted great interest as H_2-vectors for chemical hydrogen storage,[1] most recently revived by reports on the regeneration of spent fuel.[2] Aside from energy storage applications, borane amine dehydrocoupling is also highly attractive for the synthesis of polymeric B–N-materials.[3] The exothermic nature of AB dehydrogenation renders thermal degradation the simplest approach.[1] However, the onset of H_2 release is difficult to control, and the polymeric dehydrocoupling products are generally structurally ill-defined solids with varying degrees of dehydrogenation and cross-linking.[3,4] Alternatively, catalysis offers in principle the possibility of enhanced control over H_2-release kinetics and polymer microstructure. Hence, considerable efforts have been made to develop protocols for the dehydrocoupling of parent AB and of primary and secondary borane-amine adducts, using Brønsted acids and bases, Lewis acidic main group metal compounds, or frustrated Lewis acid-base pairs as catalysts.[5,6,7,8] However, most work was arguably dedicated to the application of a wide range of homogeneous transition metal catalysts, such as group 4 metallocenes,[9] group 5-7 carbonyl and nitrosyl complexes,[10] and particularly late transition metal phosphine, carbene, or olefin complexes.[11,12,13,14]

At this point, detailed mechanistic understanding will be crucial for rational catalyst design and the optimization of selectivities with respect to the formed B–N materials. However, despite all efforts in catalyst development mechanistic understanding remains limited. Most information is available for Rh, Ir, and Ru $[M(L)_2]^{n+}$-based precatalysts bearing non-chelating, bulky phosphine or N-heterocyclic carbene ligands (n = 1: M = Rh, Ir; L = P*i*Pr$_3$, P*i*Bu$_3$, PCy$_3$, IMes / n = 0: M = Ru; L = PCy$_3$). The coordination chemistry of these metal fragments with borane-amines or dehydrogenation and dehydrocoupling products, such as aminoboranes or diborazanes (H_2B–NR_2, $H(H_2B$–$NR_2)_nH$; R = H, Me; n = 1, 2), was examined by several groups.[15] Such model compounds feature B–H interactions with the metal center[16] and B–H oxidative addition has also been directly observed.[17] In contrast, experimental information about the N–H activation step is less well-established. Overall, experimental and theoretical mechanistic studies for these catalysts are in favor of pathways with formal oxidation

state change upon hydrogen transfer to the metal and aminoborane release, followed by H_2 reductive elimination.[18] To date, this mechanistic work is mostly limited to the dehydrogenation of $Me_2HN–BH_3$ (Me_2AB) which forms linear diborazane $Me_2HN–BH_2–NMe_2–BH_3$ as an intermediate and soluble *cyclo*-diaminoborane $(Me_2N–BH_2)_2$ as the final product. In comparison, dehydrocoupling of AB or $MeH_2N–BH_3$ (MeAB) and AB/MeAB co-dehydropolymerization with several catalysts was shown to give linear and/or cyclic polyaminoboranes $(RHN–BH_2)_n$ (R = H, Me) of medium to high molecular weight,[13c,13d,19] often with low solubility, thereby hampering examination. However, these results and the recent synthesis of parent $H_3N–BH_2–NH_2–BH_3$[20] fuel speculation about the relevance of linear oligoborazane intermediates for parent AB dehydrocoupling, as well.

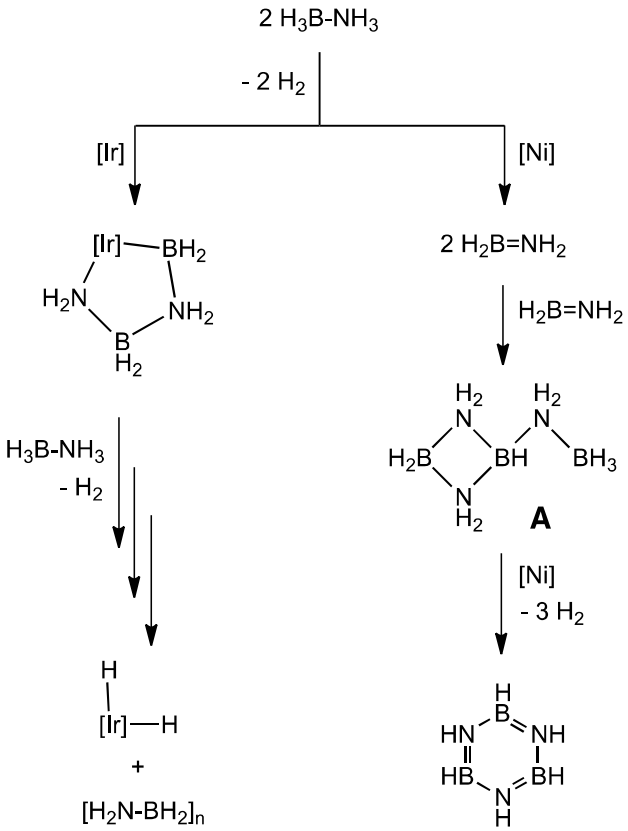

Scheme 1. Proposed pathways for the formation of AB dehydrocoupling products with Goldberg and Heinekey's Ir-catalyst and Baker's Ni-catalyst, respectively.

An elegant experimental study for this catalyst type suggested, not only for dehydrogenation but also the B–N coupling step to be a metal mediated process.[18c] Also the kinetics of AB and MeAB dehydropolymerization with a related Ir pincer catalyst support a chain growth mechanism, hence

indicating catalyzed B–N bond formation.[13d] In contrast, metal centered B–N bond formation was considered to be unlikely in a theoretical study.[21] Baker, Dixon, and co-workers proposed that the selectivity of AB dehydropolymerization depends on the fate of intermediate aminoborane:[14b] On one hand, the release of more than two equivalents of H_2, e.g. by a Ni catalyst,[14a,22] was attributed to the formation of free aminoborane $H_2N–BH_2$, a highly reactive molecule which readily oligomerizes via cyclic dehydrotrimerization product $H_3B–H_2N–B_2N_2H_7$ (**A**), ultimately giving polyborazylene after further dehydrocoupling steps (Scheme 1).[23,24,25] On the other hand, catalyst [IrH_2(POCOP)] (POCOP = C_6H_3-1,3-(OP*t*Bu_2)$_2$), produces polyaminoborane and one equiv. H_2. The absence of **A** and aminoborane trapping products was rationalized with the assumption that $H_2N–BH_2$ is bound during catalysis (Scheme 1), also explaining polymer chain growth observed with this system. This model is of fundamental importance for both hydrogen storage and B–N polymer formation:

1. It provides a rationale for the strongly differing yields in H_2.

2. A metal centered B–N coupling process enables control over the polymer microstructure by catalyst design.

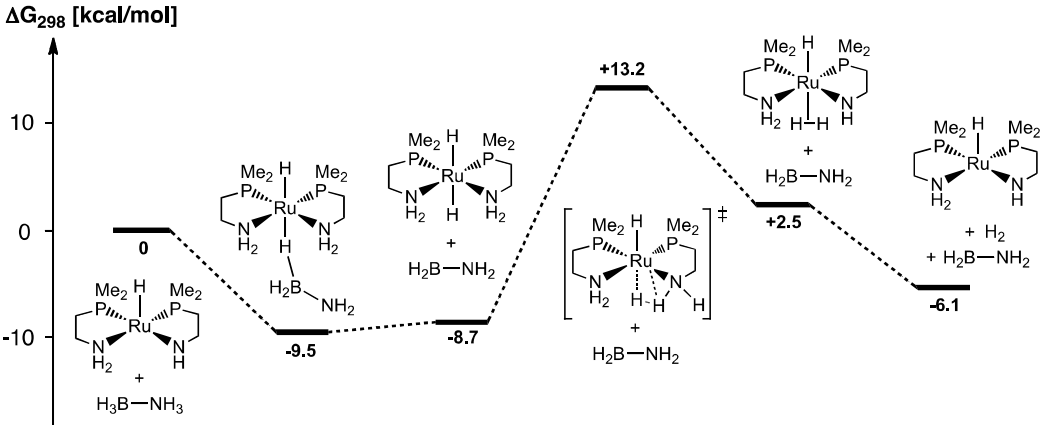

Scheme 2. Fagnou's mechanism proposed for bifunctional AB dehydrogenation.

Particularly rapid dehydrogenation of AB and MeAB was reported for ruthenium and most recently also iron precatalysts bearing potentially cooperative ligands.[11a,13d,26,27,28,29,30] For example, Williams and co-workers used Shvo's catalyst for rapid release of 2 equiv. H_2 and formation of borazine.[29] The zero order kinetics in AB for hydrogen evolution were rationalized by turn-over limiting H_2 elimination

from the catalyst after rapid outer-sphere transfer of hydrogen from the substrate and release of aminoborane. However, the product of aminoborane dehydrooligomerization, borazine, serves as a reversible catalyst poison slowing down catalysis, which could be circumvented with a related second generation catalyst.[30] In comparison, Fagnou and co-workers reported extraordinary activities in AB dehydrogenation using catalyst $[Ru(Cl)_2(iPr_2PCH_2CH_2NH_2)_2]$ and 30 equiv. of base (KO*t*Bu) as activator.[26a] Supported by DFT calculations, the authors proposed a catalytic cycle based on the assumption that the catalytically active hydrido amido complex $[Ru(H)(iPr_2PCH_2CH_2NH)(iPr_2PCH_2CH_2NH_2)]$ is formed upon activation (Scheme 2). The proposed cycle can be broken down into two parts: 1. Hydrogen transfer from the substrate to the amido catalyst in two steps with release of free $H_2N–BH_2$ and formation of dihydrido amine complex $[Ru(H)_2(iPr_2PCH_2CH_2NH_2)_2]$. 2. Subsequent turn-over limiting H_2 elimination from the resulting hydrido amine species.

Independently, our group used amido catalyst $[RuH(PMe_3)(PNP)]$ (**1**, PNP = $N(CH_2CH_2PiPr_2)_2$, Scheme 4) for AB and Me_2AB dehydrogenation (1 equiv. H_2) with comparable rates as Fagnou's catalyst.[26b,31] A bifunctional mechanism in analogy to Fagnou's proposal was considered and indicated by the kinetic isotope effects found for deuterated AB. However, the first order rate dependence on substrate excludes intramolecular H_2 elimination from the corresponding amine complex $[Ru(H)_2(PMe_3)(HPNP)]$ (**2**, Scheme 4) to be turn-over limiting, as suggested by the computations for Fagnou's system. Furthermore, experimental examination of the H_2 elimination/addition equilibrium of **1** and **2** indicated that this reaction is too slow to be relevant for AB dehydrogenation.[26b,32] However, Brønsted acid catalysis for H_2 elimination was observed and attributed to a proton-shuttle mechanism.[33] Accordingly, Nguyen and co-workers proposed a mechanism for AB dehydrogenation with our system in a computational study with strongly truncated model catalysts which picks up this idea (Scheme 3):[34] Proton transfer to the hydride ligand of $\mathbf{2^H}$ exhibits low barriers by proton shuttling with the substrate. Further, they proposed attack of hydridic B–H at the PNP amine proton with release of H_2 and aminoborane. Another equivalent of dihydrogen can then be eliminated from the resulting dihydrogen

complex without a barrier to give amido complex $\mathbf{1^H}$. Although the regeneration of $\mathbf{2^H}$ from $\mathbf{1^H}$ was not explicitly calculated to complete the catalytic cycle, transfer of hydrogen from the substrate, as in Fagnou's mechanism, seems to be a viable path at low energetic cost.

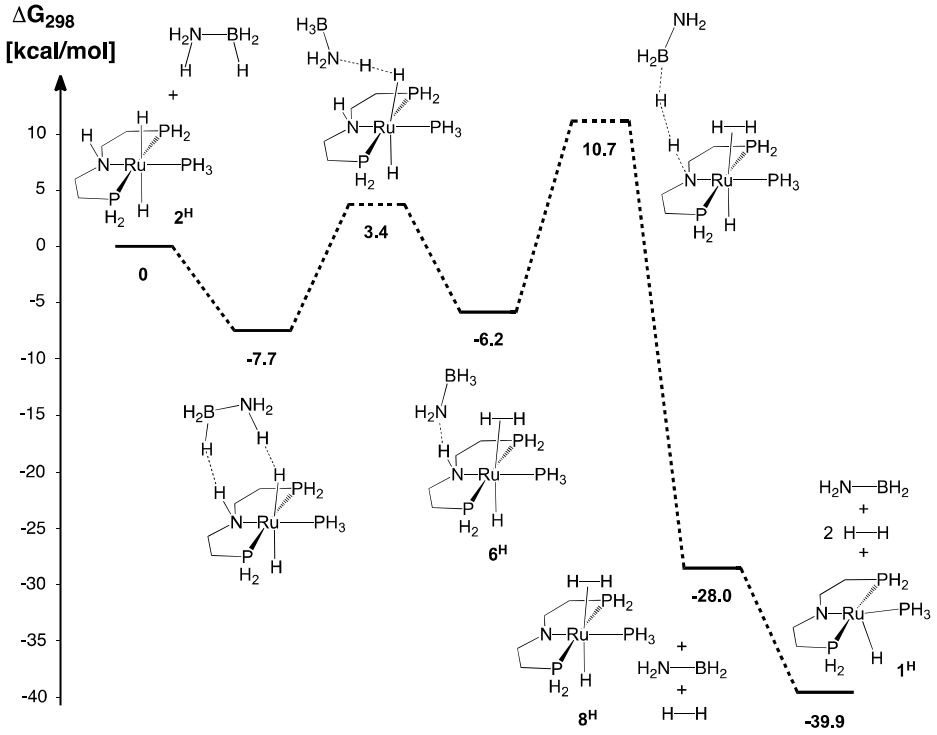

Scheme 3. Nguyen's mechanism proposed for bifunctional AB dehydrogenation.

In this paper, we report an experimental and computational study to clarify the mechanism of AB dehydrogenation with bifunctional ruthenium amine and amido catalysts. We will show that some of our experimental results are incongruent with either Fagnou's or Nguyen's proposals, leading to a modified mechanism which accounts for both dehydrogenation and B–N coupling.

RESULTS

In the first section, we describe the H_2 release kinetics for the potentially bifunctional amido and amine precatalysts [RuH(PMe_3)(PNP)] (**1**, section 1.1) and [Ru($H)_2$(PMe_3)(*H*PNP)] (**2**, section 1.2) including H/D kinetic isotope effects for the four substrates H_3N–BH_3, H_3N–BD_3, D_3N–BH_3, and D_3N–BD_3. Qualitative comparison with the structurally related (yet inherently not bifunctional) precatalyst [Ru($H)_2$(PMe_3)(*Me*PNP)] (**3**), is given in section 1.3. In section 2 the kinetic studies are complemented by stoichiometric experiments to examine substrate/catalyst interaction (section 2.1) and possible

pathways of B–N coupling, i.e. aminoborane *head-to-tail* coupling vs. intermediate release of aminoborane (sections 2.1 and 2.2). These mechanistic examinations in combination with the structural characterization of the aminoborane polymer (section 3) afford a mechanistic proposal, which differs from the previously proposed mechanisms,[26a,34] and is evaluated computationally in section 4.

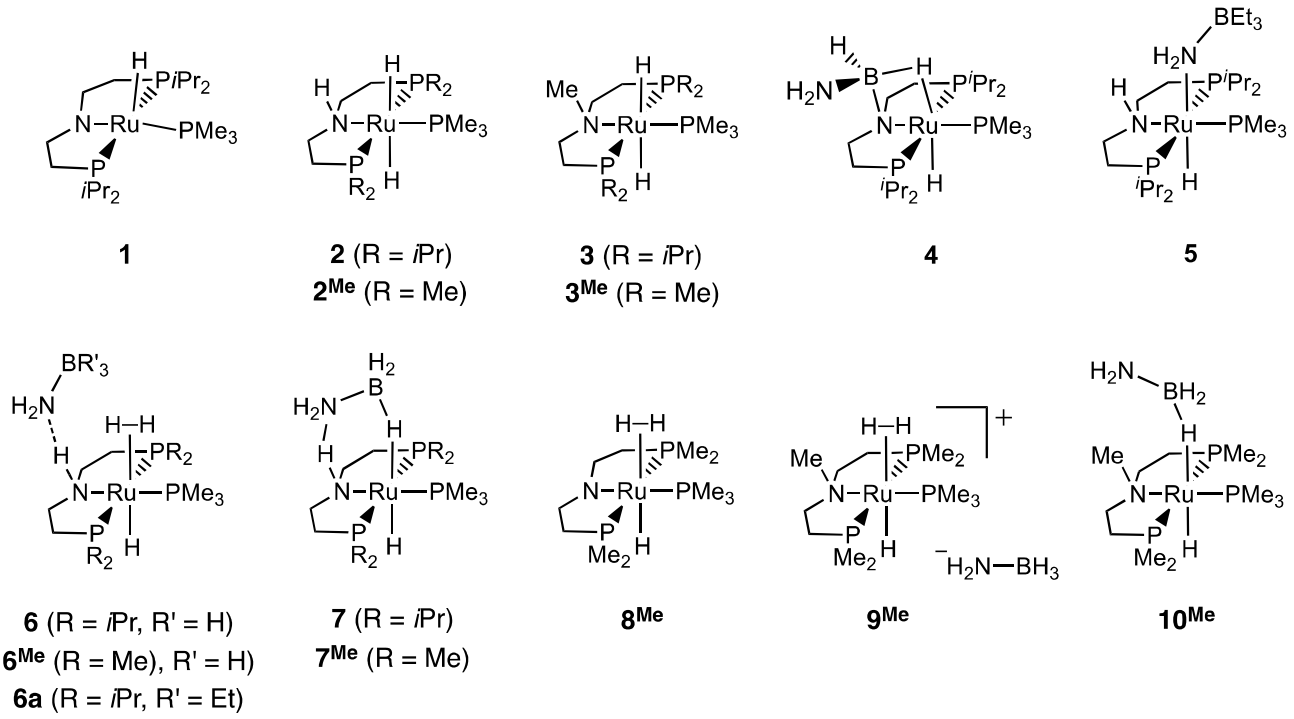

Scheme 4. Ruthenium PNP complexes discussed throughout the manuscript.

1. Kinetic studies. 1.1 Dehydrocoupling of AB with [RuH(PMe$_3$)(PNP)] (1). Addition of **1** to a solution of AB results in rapid and vigorous evolution of H_2 and precipitation of a colorless dehydrocoupling product (Scheme 5). Initial results on AB dehydrogenation using precatalyst **1** with turnover numbers (TONs) up to 8300 and turnover frequencies (TOF) around 20 s^{-1} were reported in a preceding communication.[26b] In the present study, the substrate ($[AB]_0$ = 0.25 – 2.5 M) and catalyst loadings (0.01 – 0.1 mol-%) were varied over a much wider range, with TONs ≥ 10000 at max. $[AB]_0$ / [**1**] ratios (Supporting Information Figure S1). H_2 release up to slightly more than one equiv. $[AB]_0$ suggests the formation of mostly polyaminoborane, i.e. in agreement with the polymer characterization (section 3).[35] After release of around 1 equiv. H_2, the substrate is fully consumed (solution ^{11}B NMR) and minor amounts of **A** and borazine are observed, which correlate well with the excess H_2 yield

(internal standard $NaBPh_4$), indicating decent error margins for this setup. Higher catalyst loadings result in the formation of more borazine at identical initial substrate concentrations $[AB]_0$. At high substrate conversions, catalyst deactivation product **4** (Scheme 4) is observed by ^{1}H and ^{31}P NMR spectroscopy.[31]

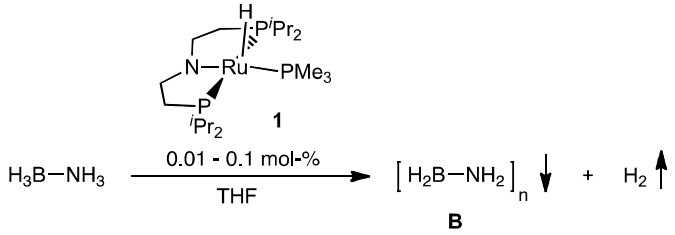

Scheme 5. Dehydrocoupling of AB with catalyst **1**.

^{11}B NMR monitoring of the reaction in a sealed (*J-Young*) NMR tube reveals considerably slower rates than volumetric (H_2) derivation. Hence, reaction rates were measured eudiometrically at room temperature and the rate law was derived from initial rates to avoid inhibition due to H_2 build-up and diffusion problems owing to product precipitation and to minimize error attributable to borazine formation at a later stage of the reaction. The data (Figure S1, Supporting Information) are in agreement with a simple rate law that is first order both in [AB] and [**1**]:

$$r_{H2} = k_{obs\mathbf{1}}[\mathbf{1}]_0[AB] \qquad \text{(Eq. 1)}$$

Accordingly, first order plots (ln[AB] *vs.* time) were also linear over two half-lifes for a wide range of catalyst and initial substrate concentrations (Figure S1, Supporting Information). Low catalyst loadings (0.05 mol-%) gave rate constants around $k_{obs\mathbf{1}} = 15 \pm 2\ M^{-1}s^{-1}$ (Table S1), in excellent agreement with the initial rate estimate ($k_{\mathbf{obs1}} = 13\ M^{-1}s^{-1}$). Higher rate constants up to $32\ M^{-1}s^{-1}$ were obtained for higher catalyst loadings (0.25 mol-% and 0.1 mol-%) (Table S1), coinciding with larger amounts of borazine being observed.

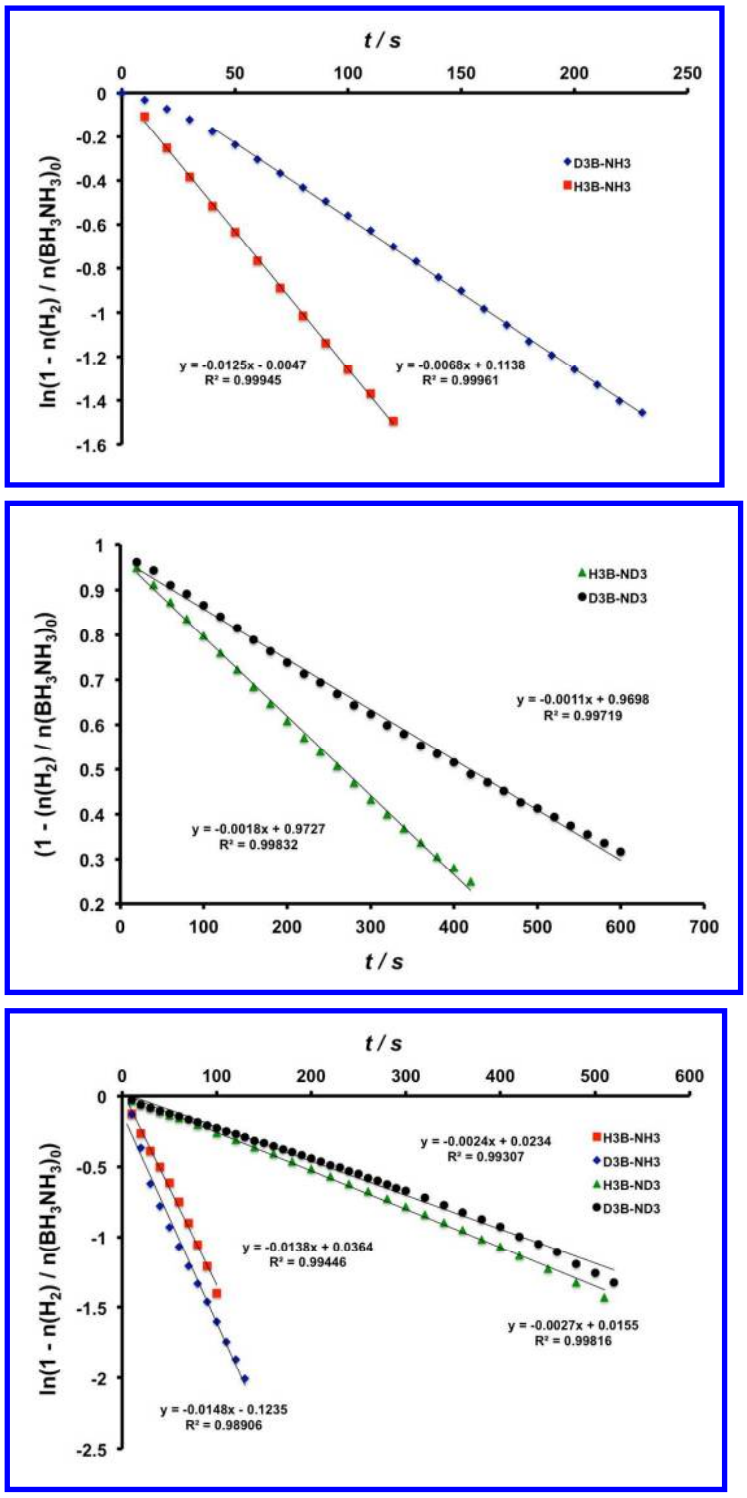

Figure 1. Kinetic isotope effects for catalysts **1** and **2**. **Top:** First order plot of $H_3N–BH_3$ and $H_3N–BD_3$ ($[AB]_0$ = 0.54 M; $[\mathbf{1}]_0$ = 0.0005 M) dehydrogenation. **Center:** Zero order plot of $D_3N–BH_3$ and $D_3N–BD_3$ ($[AB]_0$ = 0.54 M; $[\mathbf{1}]_0$ = 0.0005 M) dehydrogenation. **Bottom:** First order plot of $H_3N–BH_3$, $D_3N–BH_3$, $D_3N–BD_3$ (all: $[AB]_0$ = 0.5 M; $[\mathbf{2}]_0$ = 0.0005 M), and $H_3N–BD_3$ ($[AB]_0$ = 1.0 M; $[\mathbf{2}]_0$ = 0.001 M) dehydrogenation.

In our preceding communication, kinetic isotope effects (KIEs) for this reaction were estimated from first-order plots using *B*- (H_3N–BD_3) and *N*-terminally (D_3N–BH_3) deuterated substrates and fully deuterated D_3N–BD_3, respectively.[26b] While the experimental results were reproduced in the present study, reevaluation of the data indicated a more complex picture. As for parent H_3N–BH_3 (0.54 M; 0.1 mol-% [**1**]), the rate law for isotopomer H_3N–BD_3 exhibits first-order rate dependence on substrate over more than 2 half-lifes after a short initiation period with a KIE $k(H_3N–BH_3) / k(H_3N–BD_3) = 1.8$ (Figure 1, top).[36] However, for the *N*-deuterated D_3N–BH_3 and D_3N–BD_3, [AB] *vs.* time plots are linear over two half-lifes indicating zero order dependence of the rate law on substrate concentration (Figure 1, center), and hence a different turnover limiting step for these isotopomers. Therefore, KIE's for these isotopomers referenced to unlabeled H_3N–BH_3 could not be derived.

1.2 Dehydrocoupling of AB with [Ru(H)$_2$(PMe$_3$)(*H*PNP)] (2). Both Fagnou's (Scheme 2) and Nguyen's (Scheme 3) mechanistic proposals involve both dihydrido amine and the hydrido amido complexes as active catalyst within the catalytic cycles. Hence, complex **2** was employed as catalyst (Scheme 6) over a wide range of initial substrate concentrations $[AB]_0$ (0.25 – 1.5 M) and catalyst loadings $[Ru]_0$ (0.02 - 0.1 mol-%) (Figure S2). Since catalyst **2** is not isolable owing to facile H_2 loss,[32b] a stock solution was freshly prepared prior to every kinetic run by *in situ* hydrogenation of **1**. As for **1**, initial rates of H_2 evolution (Figure S2) are in agreement with first order dependence of the rate law in catalyst and substrate (Eq. 2):

$$r_{H2} = k_{obs2}[\mathbf{2}]_0[AB] \qquad \text{(Eq. 2)}$$

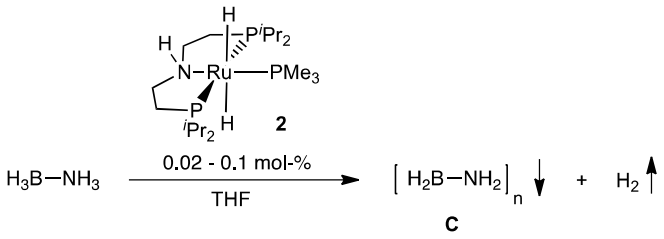

Scheme 6. Dehydrocoupling of AB with precatalyst **2**.

A rate constant $k_{obs2} = 24 \pm 2$ $M^{-1}s^{-1}$ was estimated, i.e. higher than for precatalyst **1** ($k_{obs1} = 13$ $M^{-1}s^{-1}$). First order plots (ln[AB] *vs.* time) were also linear over approximately two half-lifes for an even larger

range of catalyst and substrate initial concentrations, as compared with precatalyst **1** (Supporting Information). The rate constant extracted from these plots (k = 22 $M^{-1}s^{-1}$, Figure S2) is in excellent agreement with the initial rate estimate indicating that the simple rate law (Eq. 2) is applicable over large parts of the catalytic reaction.

As for precatalyst **1**, KIEs were derived with isotopically labeled substrates. However, with **2** all isomers ($H_3N–BH_3$, $H_3N–BD_3$, $D_3N–BH_3$, $D_3N–BD_3$) exhibit first order rate dependence on [AB] (Figure 1 bottom). Also in contrast with **1**, *B*-terminal deuteration resulted in no KIE ($k(H_3N–BH_3)$ / $k(H_3N–BD_3)$ = 1.0; $k(D_3N–BH_3)$ / $k(D_3N–BD_3)$ = 1.1). Large KIEs were obtained for the *N*-terminally deuterated isotopomers ($k(H_3N–BH_3)$ / $k(D_3N–BH_3)$ = 5.3; $k(H_3N–BH_3)$ / $k(D_3N–BD_3)$ = 5.9). These results indicate N–H bond cleavage, yet no B–H activation in the turnover limiting step and will be analyzed in combination with the computational results in the discussion section.

1.3 Dehydrocoupling of AB with [Ru(H)$_2$(PMe$_3$)(*Me*PNP)] (3). To further probe for the potential relevance of ligand cooperativity, tertiary amine complex [Ru(H)$_2$(PMe$_3$)(*Me*PNP)] (**3**)[33] was employed as a reference catalyst (Scheme 7 and Figure S3). Methylation of the pincer ligand nitrogen atom prohibits N–H bonding. Thus, a bifunctional mechanism cannot be operative for this catalyst. Addition of **3** to a solution of AB in THF at room temperature results in evolution of H_2 and precipitation of the polymeric dehydrocoupling product **D**. As for catalysts **1** and **2**, high turnover numbers (TON ≥ 10000 at $[AB]_0$ = 2.5 M and $[\mathbf{3}]_0 = 1 \cdot 10^{-4}$ M) were observed. However, the rate of H_2 evolution is considerably lower by almost two orders of magnitude (Figure 2), as compared with compounds **1** and **2**. Initial rates for a wide range of substrate concentrations ($[AB]_0$ = 0.25 M – 2.5 M) and catalyst loadings (0.05 mol-%, 0.10 mol-%, 0.25 mol-%) also indicate first order dependence of the rate law in both catalyst and substrate (Figure S3):

$$r_{H2} = k_{obs3}[\mathbf{3}]_0[AB] \qquad \text{(Eq. 3)}$$

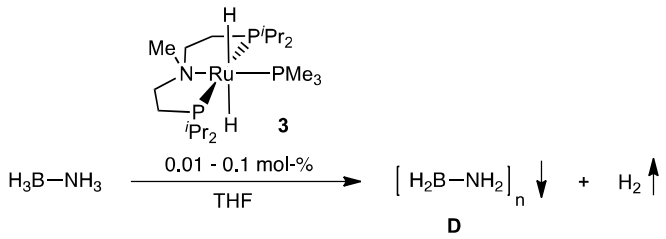

Scheme 7. Dehydrocoupling of AB with precatalyst **3**.

The rate constant derived by the initial rate method (k_{obs3} = 0.6 $M^{-1}s^{-1}$) is slightly smaller as compared with the rate constant obtained from first-order plots (0.9 ± 0.3 $M^{-1}s^{-1}$, Figure S3), yet within statistical error.[37,38] The first-order plots generally showed good linearity over two half-lives, suggesting that the dehydrocoupling mechanism does not substantially change over the course of the reaction.

2. Stoichiometric examinations. 2.1 Reactions with model substrates. The reactions of catalysts **2** and **3** with model substrates $H_3N–BEt_3$ and $Me_3N–BH_3$ were investigated by NMR spectroscopy. Blocking of the *B*- or *N*-termini, respectively, by full substitution enabled the examination of initial substrate interactions with the catalyst without dehydrocoupling. An equimolar mixture of **2** or **3** with $Me_3N–BH_3$ did not reveal any reaction on the NMR timescale, as judged by ^1H, ^{31}P, ^{11}B, and ^1H 2D EXSY NMR spectroscopy. In contrast, a mixture of **2** and $H_3N–BEt_3$ (1.5 equivalents in THF) exhibits a small equilibrium concentration (< 10 %) of a new compound. This compound could not be isolated, but was assigned to borane amido complex **5** (Scheme 8). Its spectroscopic data are in agreement with the meridional arrangement of three phosphine ligands (^{31}P NMR), a single hydride ligand (–18.4 ppm), which is in *trans*-position to a boraneamido and *cis*- with respect to the phosphine ligands, and with further signals assignable to a $H_2N–BEt_3^-$ ligand. Most importantly, the ^1H 2D EXSY NMR spectrum of this mixture reveals stereoselective exchange of the $H_3N–BEt_3$ N–H protons with the hydride ligand of **2** that is in *syn*-position to the pincer N–H proton (Figure S5). Quantification of the exchange rates was not possible, due to peak overlaps. However, this result is in agreement with an exchange mechanism via transient dihydrogen complex **6a** (Scheme 8), which can form the minor equilibrium concentration of **5a** upon loss of H_2. The stereoselectivity of the N–H/Ru–H exchange is indicative of the stabilization of **6a** by hydrogen bonding, as previously proposed for proton exchange of **2** with water.[33] Similarly, for

a mixture of $H_3N–BEt_3$ and **3** new NMR signals in the ^{31}P and ^{1}H (–19.7 ppm) NMR spectra were assigned to the formation of around 10% of an amido complex [Ru(NH_2BEt_3)(H)(PMe_3)(*Me*PNP)]. However, no N–H/Ru–H exchange was detected on the NMR timescale of EXSY NMR experiments (τ_m^{max} = 1000 ms). Hence, hydride exchange with the substrate protons must proceed at considerably slower rates as compared with complex **2**.

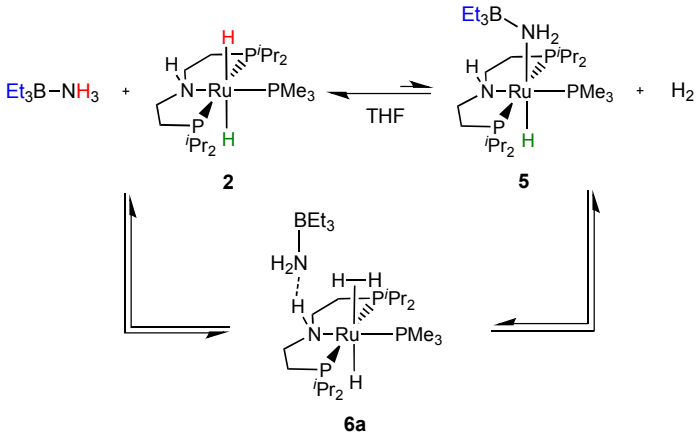

Scheme 8. Reaction of **2** with $H_3N–BEt_3$ and proposed mechanism via dihydrogen complex **6a**. Colors indicate selected chemical exchange cross peaks observed by ^{1}H 2D EXSY NMR.

A possible pathway for the formation of linear products, such as polyaminoboranes $H_3N–(H_2N–BH_2)_n–BH_3$, could be the direct head-to-tail dehydrocoupling of two borane-amine substrate molecules. Hence, $Me_3N–BH_3$ and $H_3N–BEt_3$ were used as model substrates within a cross-coupling experiment in the presence of catalyst **2** (1.0 mol-%). Over several hours at room temperature no coupling reaction was observed by ^{11}B NMR (Scheme 9), indicating, that proton and hydride transfer from the same substrate molecule to the catalyst is required. Furthermore, substrate metathesis by B–N bond cleavage can be excluded.

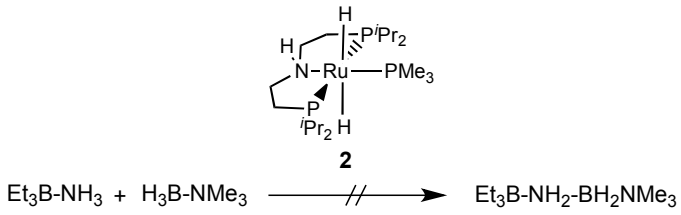

Scheme 9. Cross-coupling experiment of $Me_3N–BH_3$ and $H_3N–BEt_3$ in the presence of **2**.

2.2 Aminoborane trapping experiments. As a result from the cross-coupling experiment, H_2 seems to be transferred from the same substrate molecule to the catalyst. Hence, the release of free aminoborane $H_2N–BH_2$ within the mechanism was probed by trapping experiments with cyclohexene, as introduced by Baker and co-workers.[14b] AB dehydrocoupling with precatalyst **1** in the presence of cyclohexene (21 equivalents with respect to AB) showed no olefin hydroboration products (^{11}B NMR) within the timescale of the dehydrocoupling reaction (full substrate consumption by ^{11}B NMR). Importantly, only small amounts of polyborazylene and borazine were detected. However, after 20 h at room temperature, rising amounts of borazine and trapping product $H_2N–B(C_6H_{11})_2$ (^{11}B NMR: δ = 48.4 ppm)[39] were observed, indicating rearrangement processes, such as slow degradation of the initially formed, insoluble polyaminoborane. Similarly, trapping experiments with catalyst **2** gave besides insoluble polyaminoborane some polyborazylene and borazine by ^{11}B NMR. No trapping products from cyclohexene hydroboration were initially observed, but small amounts were detected 24 h after completion of the dehydrogenation, as similarly found for **1**. These results for catalysts **1** and **2** contrast with trapping experiments for catalyst **3**. In this case, not only borazine and small amounts of **A** are observed in solution, but also considerable amounts of $H_2N–B(C_6H_{11})_2$ within the timescale of the dehydrogenation reaction (Figure S4), indicative of the release of free aminoborane.

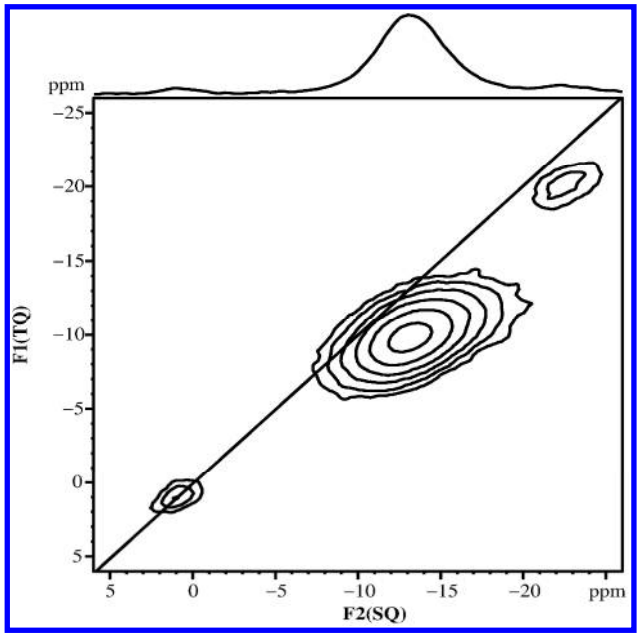

Figure 2. ^{11}B MAS NMR sheared triple-quantum filtered MQMAS spectrum of polymer **C**.

3. Polymer Characterization. The white, insoluble products resulting from AB dehydrocoupling were further examined. Characterization of **B** by IR and solid-state ^{11}B MAS spectroscopy was reported in a preceding communication.[26b] Combustion analysis and IR spectra of **C** and **D** are in agreement with the formation of the same product as obtained with catalyst **1** or with an Ir(POCOP) catalyst,[13c,13d,26b] assignable to polyaminoborane $H_3N–(BH_2–NH_2)_n–BH_3$, rather than the originally proposed cyclic pentaaminoborane $(H_2N–BH_2)_5$.[13a] As was previously found, some solvent adheres to the polymer even after extended drying in vacuo, which was also observed with other catalysts.[13c,d] For example, elemental analysis of **D** supports the formation of $H_3N–(BH_2–NH_2)_{19}–BH_3 \cdot 0.6$ THF, as similarly reported for AB dehydrocoupling with an Ir(POCOP) catalyst by Staubitz et al. ($n \approx 20$).[13d] In this study, ^{11}B Multiple-Quantum Magic-Angle-Spinning (MQMAS) NMR spectroscopy was emphasized to determine the isotropic chemical shift and differentiate between true resonances and second-order quadrupole line shapes. The ^{11}B MQMAS NMR spectrum of **B** (Figure S7) features two signals, one of higher intensity at δ_{iso} = –10.7 ppm (second-order quadrupolar effect (SOQE) = 1.5 MHz) and one of lower intensity at δ_{iso} = –21.0 ppm (SOQE = 1.4 MHz). These peaks indicate two different boron environments present in the polymer, assignable to linear main chain BH_2 groups and terminal BH_3 end groups, respectively, by comparison with soluble boranes, such as AB ($\delta(^{11}B)$ = –23 ppm)[40] or $H_3N–BH_2–NH_2–BH_3$ ($\delta(^{11}B)$ = –11.6 (BH_2) and –22.8 ppm (BH_3)).[20] While the ^{11}B spectrum of **B** considerably differs from early reports of polyaminoborane,[41] it is almost identical with the polyaminoborane prepared by Ir(POCOP)-catalyzed AB dehydrocoupling.[13d] Similarly, the ^{11}B MQMAS NMR spectrum of polymer **C** (Figure 2) exhibits a low intensity signal at δ_{iso} = –21.0 ppm (BH_3, SOQE = 1.3 MHz) and the main signal at δ_{iso} = –11.1 ppm (BH_2, SOQE = 1.5 MHz). In addition, a small signal at δ_{iso} = 1.0 ppm (SOQE < 0.4 MHz) is observed. This signal, yet even weaker, is also visible in polyaminoborane obtained with the Ir(POCOP) catalyst, but absent in **B**. Owing to its chemical shift (e.g. $Li[B(NHMe)_4]$: $\delta(^{11}B)_{THF}$ = 0.2 ppm)[42] and small SOQE, which indicates a highly

symmetric (tetrahedral) environment around the boron atom, this peak is assigned to $B(NH_2)_4$ moieties within the polymer indicating some crosslinking of the chains.

4. DFT computations. 4.1 Dehydrogenation with model catalyst 2^{Me}. Our mechanistic proposal for AB dehydrocoupling with PMe_2-truncated model catalysts $\mathbf{2}^{Me}$ and $\mathbf{3}^{Me}$ was evaluated using density functional theory (DFT, B3LYP/6-31+G**). The overall dehydrogenation reaction of AB to H_2 and aminoborane was calculated to be exergonic by $\Delta G^0 = -16.5$ kcal/mol (Scheme 10), only slightly larger than previously reported results at a much higher level of theory (–12.4 kcal/mol; MP4/++3df).[43]

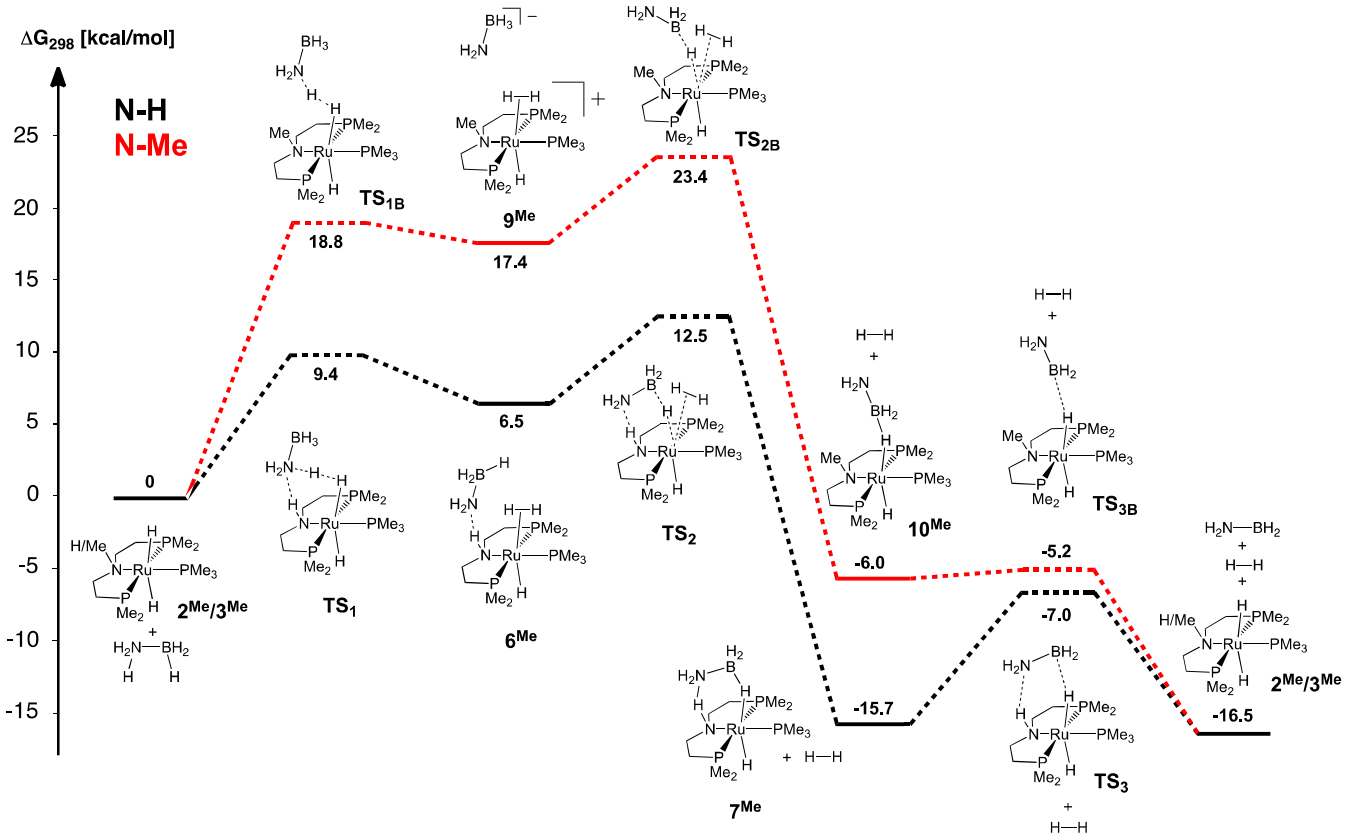

Scheme 10. DFT results for the proposed mechanism of AB dehydrogenation, catalyzed by $\mathbf{2}^{Me}$ (black line) and $\mathbf{3}^{Me}$ (red line), respectively.

The calculated mechanism for catalyst $\mathbf{2}^{Me}$ was guided by the experimental results presented above. Initial interaction of $\mathbf{2}^{Me}$ with the *N*-terminal protons of AB leads to dihydrogen complex $\mathbf{6}^{Me}$ and is endergonic by $\Delta G^0 = +6.5$ kcal/mol. Formation of the H_2 ligand (D(H–H) = 0.80 Å) is accompanied by a hydrogen bridge within the ion pair ($D(H_3BH_2N–H)$ = 1.70 Å; $D(N^{PNP}–H)$ = 1.09 Å). This

stabilization results in an energetically considerably more favorable pathway as compared with catalyst $\mathbf{3^{Me}}$ (see below). Formation of the heavily truncated model complex $\mathbf{6^{H}}$ was calculated by Nguyen *et al.* to be even exergonic by ΔG^0 = –6.2 kcal/mol. However, such strong stabilization is not in agreement with our EXSY NMR studies for the real system (section 2.1).[34] Transition state $\mathbf{TS_1}$ is late on the reaction coordinate according to bond lengths (D(H_3BH_2N–H) = 1.82 Å; D(H–H) = 0.84 Å).

Concerted hydrogen loss and borane attack within $\mathbf{6^{Me}}$ via $\mathbf{TS_2}$ gives cyclic aminoborane adduct $\mathbf{7^{Me}}$. According to bond distances, the bridging hydride ligand is firmly bound to both the aminoborane (D(B–HRu) = 1.31 Å) and the metal center (D(Ru–HB) = 1.83 Å), while the bridging amine proton is only weakly hydrogen bound to the aminoborane (D(N^{PNP}–H) = 1.05 Å; D($H_2BH_2N\cdots HN^{PNP}$) = 1.83 Å). However, both N and B atoms of the aminoborane are strongly pyramidalized. H_2 release is irreversible (ΔG^0 = –22.2 kcal/mol) and also accompanied by a low kinetic barrier ($\Delta G^{\ddagger}$($\mathbf{TS_2}$) = 6.0 kcal/mol). In the transition state ($\mathbf{TS_2}$), the H_2 ligand is almost completely cleaved from the metal center (D(Ru–H) = 2.80 and 2.81 Å; D(H–H) = 0.75 Å) while the approach of the borane moiety is only completed to a small extend (D(Ru–HB) = 3.16 Å). H_2-loss represents the highest overall point on the potential Gibbs energy surface within the catalytic cycle. Hence, this step and the pre-equilibrium of H_2-complex formation should be turn-over limiting. Isotope effects for substrate H/D isotopomers were also computed and will be compared with experimental values in the discussion section.

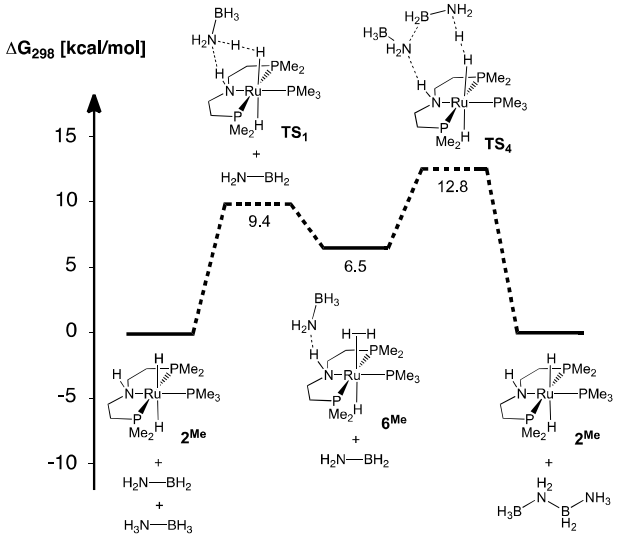

Scheme 11. DFT results for the proposed mechanism of catalyzed B–N coupling.

An alternative pathway to concerted H_2-loss and borane attack via TS_2 would be a stepwise mechanism. In fact, a pathway through dihydrogen amido complex $\mathbf{8^{Me}}$ (Scheme 4),[33] which loses H_2 and is subsequently attacked by AB was located and the minimum barriers for the two sequences $\mathbf{2^{Me}}$ + AB $\rightarrow$ $\mathbf{8^{Me}}$ + AB $\rightarrow$ $\mathbf{1^{Me}}$ + H_2 + AB $\rightarrow$ $\mathbf{7^{Me}}$ + H_2 (stepwise) and $\mathbf{2^{Me}}$ + AB $\rightarrow$ $\mathbf{6^{Me}}$ $\rightarrow$ $\mathbf{7^{Me}}$ + H_2 (concerted) are within a few kcal/mol and therefore indistinguishable by DFT. However, with the large excess of substrate the equilibrium $\mathbf{6^{Me}}$ □ $\mathbf{8^{Me}}$ + AB will be shifted towards $\mathbf{6^{Me}}$, in favor of the concerted mechanism (Scheme 10). Furthermore, our kinetic studies suggest, that **1** and **2** do not go through the same catalytic cycle. In comparison, Nguyen and co-workers located the transition state for $\mathbf{6^{H}} \rightarrow \mathbf{8^{H}}$ + H_2 + H_2B–NH_2 in their alternative pathway at $\Delta G^{‡}$ = 16.9 kcal/mol (Scheme 3).

Finally, aminoborane elimination from $\mathbf{7^{Me}}$ restores catalyst $\mathbf{2^{Me}}$ with a small barrier ($\Delta G^{‡}(\mathbf{TS_3})$ = 8.7 kcal/mol). The long bridging B–H (2.57 Å) and N–H (2.45 Å) distances and planarity of the H_2NBH_2 moiety are indicative of a late transition state $\mathbf{TS_3}$. In contrast to catalyst $\mathbf{3^{Me}}$ (see below), this reaction is almost thermoneutral (ΔG^0 = 0.8 kcal/mol), suggesting an equilibrium for aminoborane release. However, a low energy pathway for aminoborane coupling with borane-amines to linear products was also found (see below). Hence, a low steady state concentration should arise for H_2NBH_2.

4.2 B–N coupling with model catalyst $\mathbf{2^{Me}}$ Previous studies suggested that uncatalyzed oligomerization of aminoborane results in cyclic products.[14b] Analysis of the dehydrocoupling products with catalysts $\mathbf{1^{Me}}$ and $\mathbf{2^{Me}}$ supports the formation of mainly linear polyaminoborane with minor cross-linking. The results of the cross-coupling experiments (Section 2.1) rule out the direct dehydrogenative head-to-tail-coupling of two substrate molecules. An alternative pathway is offered by coupling of aminoborane, the initial product of AB dehydrogenation, with AB (or higher, linear borane-amine adducts). A mechanism with low activation barriers was found on this route (Scheme 11). In fact, the same intermediate of the dehydrogenation cycle that results from substrate *N*-terminal activation ($\mathbf{6^{Me}}$) is attacked by aminoborane leading to the net insertion into an N–H bond. Formation of linear H_3B–H_2N–H_2B–NH_3 exhibits an almost identical barrier as H_2-loss ($\Delta\Delta G^{‡}$ = 0.3 kcal/mol), providing a model for

energetically competitive polyaminoborane enchainment. The observation of aminoborane trapping product $Cy_2B–NH_2$ several hours after consumption of the substrate can also be rationalized: According to our calculations (and others' at higher level of theory),[24] aminoborane insertion is almost thermoneutral, rendering this reaction reversible and therefore mainly driven by precipitation of the polyaminoborane from solution.

The large excess of AB at catalytic conditions raises the question whether direct reaction of AB with $\mathbf{7^{Me}}$ is possible without intermediate release of aminoborane. Several pathways were computed, such as *N*-terminal attack of AB at the bridging hydride or at the bridging proton of $\mathbf{6^{Me}}$. However, all efforts resulted in considerably higher barriers as compared with the mechanism outlined in Scheme 12. A strong energetic penalty seems to arise from the cleavage of the hydrogen bond without concerted B–H cleavage and planarization to aminoborane, and vice versa. Although we do not want to fully rule out the possibility of B–N coupling without intermediate aminoborane release, because of the lack of kinetic data, the current mechanistic model (Scheme 11) represents an upper rate limit and is in agreement with turn-over limiting hydrogen release.

4.3 Dehydrogenation with model catalyst $\mathbf{3^{Me}}$. The cooperative effect of the PNP ligand was further examined by computation of the same mechanistic pathway for catalyst $\mathbf{3^{Me}}$ (Scheme 10). Both the transition states and the dihydrogen complex intermediate that lead to hydrogen elimination are about 10 kcal/mol at higher energy compared with $\mathbf{2^{Me}}$. This result is attributed to the stabilization of the ion pair in case of **2** by hydrogen bonding with the PNP amine functional group. Hence, this effect is likely to be somewhat overemphasized within the computations, as hydrogen bonding with other substrate molecules under catalytic conditions possibly stabilizes this pathway. However, the result is in qualitative agreement with the experimental observation that **3** catalyzes AB dehydrogenation with rates almost two orders of magnitude smaller than **2**. As for $\mathbf{6^{Me}}$, H_2 release is irreversible and accompanied by formation of a hydride bridged adduct with aminoborane ($\mathbf{10^{Me}}$: *D*(B–HRu) = 1.35 Å; *D*(Ru–HB) = 1.83 Å). Owing to the terminal bonding, dissociation of aminoborane is associated with a minute barrier ($\Delta G^{\ddagger}$ = 0.8 kcal/mol) to complete the catalytic cycle.

DISCUSSION

The kinetic, spectroscopic, and computational results for the rapid AB dehydropolymerization to mainly linear polyaminoborane with our bifunctional ruthenium amine catalyst allow for the formulation of a mechanistic model. Solely based on DFT calculations, two different mechanisms for this type of catalysts had been previously proposed by Fagnou[26a] and by Nguyen,[34] respectively. However, both mechanistic proposals exhibit features which are not in agreement with some of our experimental results:

1. In Fagnou's mechanism (Scheme 2) hydrogen transfer from the substrate to the amido catalyst species was calculated to be thermodynamically downhill, followed by rate determining, intramolecular H_2 elimination. Hence, when assuming irreversible loss of gaseous H_2 in an open system, a rate law which is zero order in AB should result, as for Shvo's catalyst,[29] but first order dependence was found with our catalysts **1** and **2**.

2. Nguyen's mechanism (Scheme 3) supports an equilibrium of **2** and AB with an energetically low lying dihydrogen complex. While such an equilibrium was in fact found with model substrate $Et_3B–NH_3$ (Section 2.1) the putative dihydrogen complex **6a** is not detected by NMR, suggesting that it should be more than 10 kJ/mol higher in energy.

3. Both mechanisms propose the involvement of the respective amido and amine complexes as active species within the same catalytic cycle. However, despite very similar turn-over frequencies starting from catalysts **1** or **2**, respectively, we found considerably different kinetics for the deuterated isotopomers and different degrees of cross-linking in the resulting polyaminoboranes. These observations suggest that catalysts **1** and **2** do not catalyze AB dehydrogenation through the same mechanism.

On the other hand, some of the features within Fagnou's and Nguyen's mechanisms could be confirmed:

1. Both mechanisms include the involvement of the amine functional groups in the sense of bifunctional catalysis. Accordingly, the use of a tertiary amine ligand (catalyst **3**) results in rates that are almost two order of magnitude slower as compared with catalysts **1** and **2**.

2. Nguyen suggested, in contrast to Fagnou's mechansim, that transfer of a proton from the substrate *N*-terminus to a hydride ligand of **2** is the initial step of the catalytic cycle. We had previously demonstrated hydride protonation of **2** by other Brønsted acids with EXSY NMR spectroscopy.[33] This method similarly indicates stereoselective N–H proton exchange of model substrate $Et_3B–NH_3$ with **2**, as proposed in Nguyen's mechanism.

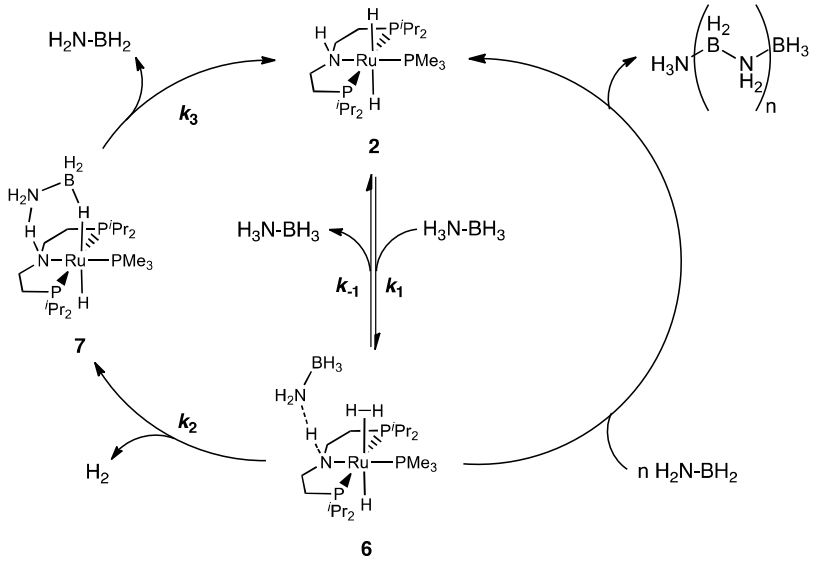

Scheme 12. Proposed mechanistic cycles for AB dehydrocoupling with catalyst **2**.

The catalytic cycle that we propose for catalyst **2** represents a modification of these two previously published mechanisms and, in addition, a pathway for polymer formation. The complete mechanism can be broken down into two connected catalytic cycles (Scheme 12): The left cycle accounts for AB dehydrogenation with release of H_2 and aminoborane $H_2N–BH_2$, respectively. The right cycle offers a route for metal-mediated oligomerization by catalytic insertion of aminoborane into a N–H bond of the substrate. The latter pathway via dihydrogen complex **6** was computed to exhibit very low barriers explaining the formation of mostly linear $H_3N–(BH_2–NH_2)_n–BH_3$. As for the Ir(POCOP) catalyst, the polyaminoborane then precipitates from solution (THF) at around n ≈ 20 (^{11}B MQ-MAS NMR

spectroscopy), thereby driving the reaction to completion. However, line shape analysis of broad, unresolved peaks exhibits relatively large uncertainty.[44] Cross-linking of the polymer to a smaller extend is also indicated by solid state NMR.

Rapid, metal-catalyzed B–N coupling with catalysts **1** and **2** also explains the trapping experiments (Scheme 13): The initial absence of cyclohexylboranes suggests that hydroboration is kinetically not competitive with B–N coupling. The calculated barriers for dehydrogenation and B–N coupling are almost identical suggesting a low steady-state concentration for aminoborane. However, the observation of the trapping product several hours after completion of the reaction can be explained by slow degradation of polyaminoborane via the reverse reaction, i.e. aminoborane extrusion from the polymer. Note that the linear diborazane $H_3N–BH_2–NH_2–BH_3$ had been reported as a stable molecule, suggesting that polymer decomposition should be a catalyzed process.[20] Furthermore, B–N coupling with catalyst **2** was not only computed to proceed with low barriers (DFT), but is also almost thermoneutral, hence reversible. In case of catalyst **3**, the relative reaction rates of B–N coupling vs. hydroboration are more in favor of aminoborane trapping, again indicating that B–N coupling is a metal-catalyzed process.

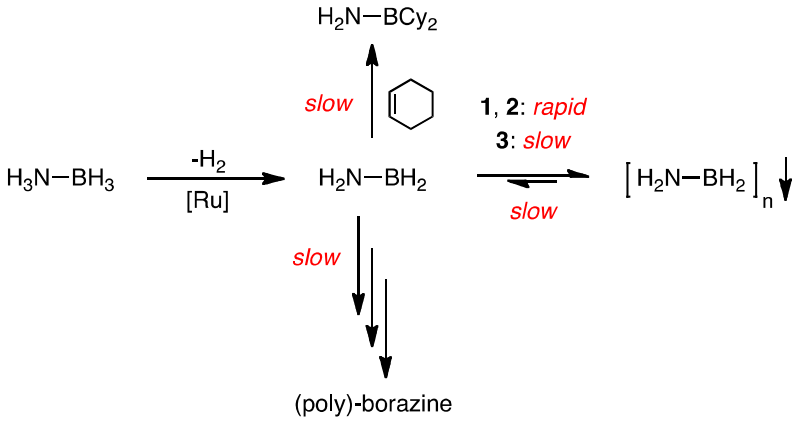

Scheme 13. Qualitative kinetic model that explains the trapping experiments.

Reversibility of the metal centered B–N coupling process was previously demonstrated by Manners and co-workers for MeAB:[45] When starting either from MeAB or from $MeH_2N–BH_2–MeHN–BH_3$ in the presence of catalyst [IrH_2(POCOP)] the polymeric dehydropolymerization product $(MeHN–BH_2)_x$ was obtained. Addition of cyclohexene, did not give any hydroboration trapping product of the free

aminoborane. Interestingly, the trapping product $MeHN–BCy_2$ was formed upon metal free, thermal degradation of $MeH_2N–BH_2–MeHN–BH_3$. These results indicate, as for catalysts **1** and **2**, that trapping by hydroboration cannot compete with catalytic B–N coupling. While the B–N coupling mechanism for the Ir(POCOP) system is not known, Weller and co-workers proposed a pathway for metal centered dehydrocoupling of two MeAB with $[Ir(H)_2(H_2)_2(PCy_3)_2]^+$ via initial B–H activation, H_2-loss, and coupling of two metal-bound fragments.[13e] Our mechanism via initial N–H activation and outer sphere coupling represents an alternative pathway.

The proposed dehydrogenation cycle (Scheme 11, left side) starts from dihydrido amine **2** to form dihydrogen complex **6** upon reaction with AB. The proton shuttle pre-equilibrium prior to irreversible loss of H_2 was calculated to go through a considerably lower kinetic barrier compared with the inherently non-bifunctional catalyst **3**. It is qualitatively supported by the rapid, stereoselective proton exchange of **2** with model substrate $H_3N–BEt_3$ (EXSY NMR). This mechanism also exhibits lower computed barriers than direct, intramolecular H_2 loss from **2**,[32,33] as proposed by Fagnou for his system. The dehydrogenation cycle is closed by aminoborane loss from complex **7**. This reaction step is assumed to be irreversible due to rapid aminoborane oligomerization as suggested by the initial absence of olefin trapping products and the computational identification of a low energy pathway for catalyzed B–N coupling. Hence, the rate law for H_2 release can be expressed as (Supporting Information):

$$r_{H2} = K_1 k_{\mathbf{2}}[\mathrm{Ru}][\mathrm{AB}] \qquad \text{(Eq. 5)}\ [46]$$

$$k_{obs\mathbf{2}} = K_1 k_{\mathbf{2}} \qquad \text{(Eq. 6)}$$

This simple kinetic model can be evaluated by comparison of the experimental isotope effects for $k_{obs\mathbf{2}}$ with the computed isotope effects for K_1k_2 for deuterated substrates $D_3B–NH_3$, $H_3B–ND_3$, and $D_3B–ND_3$. Such calculations were successfully used in the past to evaluate hydrogenation mechanisms,[47] with the advantage that relative rates are compared, rather than absolute rates. Computation of the isotope effects for fully deuterated $D_3B–ND_3$ was straightforward using $[Ru(D)_2PMe_3\{DN(CH_2CH_2PMe_2\}]$ (**d_3-2^{Me}**) as starting structure owing to the exchange of all hydrides and the amine proton within the catalytic cycle. The high computed isotope effect ($K^H_1k^H_2/K^D_1k^D_2$ = 5.6, Table 2 and Supporting Information) is

in good agreement with the experimental (k^H_{obs2}/k^D_{obs2} = 5.9) value. Likewise, *B*-terminal deuteration gives, both experimentally and computationally, no rate change (Table 1 'no scramble'). For the calculations, the reaction sequence is initiated with [Ru(D)$_2$PMe$_3${HN(CH$_2$CH$_2$PMe$_2$}] (**d$_2$-2^{Me}**), assuming regioselective transfer of B–D to Ru–D and N_{AB}–H to N_{PNP}–H, as proposed within our mechanism (Scheme 10 and Supporting Information Scheme S1). Interestingly, the computed value ($K^H_1k^H_2/K^D_1k^D_2$ = 1.0) is a combination of an inverse equilibrium isotope effect (K^H_1/K^D_1 = 0.5), which is offset by the normal KIE for HD elimination (k^H_2/k^D_2 = 2.1). However, the computed isotope effects are complex and cannot be easily rationalized, as several E–H/D (E = N, B, Ru) bonds are simultaneously formed and broken in both transition states.

Table 1. Comparison of computed and experimental isotope effects.

	$K^H_1k^H_2$ / $K^D_1k^D_2$		k^H_{obs2} / k^D_{obs2}
	no scramble	scramble	
D$_3$B–NH$_3$	1.0	1.7	1.0
H$_3$B–ND$_3$	8.2	5.3	5.3
D$_3$B–ND$_3$	5.6		5.9

The situation is more complex for *N*-deuterated substrate D$_3$N–BH$_3$. The prediction of the isotope effect by DFT with the same approach as for the isotopomer H$_3$N–BD$_3$, i.e. assuming regioselective H-transfer by using [Ru(H)$_2$PMe$_3${DN(CH$_2$CH$_2$PMe$_2$}] (**d$_1$-2^{Me}**) as starting structure (Scheme S1 'no scramble') gives a very high value ($K^H_1k^H_2/K^D_1k^D_2$ = 8.2), hence failing to reproduce the experimental result (k^H_{obs2}/k^D_{obs2} = 5.3). However, the smaller rate retardation can be rationalized by the consideration of H/D-scrambling. Our results from 2D EXSY NMR spectroscopy demonstrated rapid substrate *N*-terminal proton exchange with the catalyst hydride ligands and amine proton. This observation suggests possible H/D scrambling prior to H_2 elimination. In fact, H/D scrambling likely proceeds through the same intermediate as dehydrogenation (**6**). It is therefore reasonable to assume that scrambling is at least on the same timescale or faster as dehydrogenation. In that case, the system will then follow the lowest energy pathway out of the different possible isotopomeric distributions. Hence, the alternative pathways

with H/D scrambling prior to H_2 elimination, i.e. starting from $\mathbf{d_0\text{-}2^{Me}}$ and $\mathbf{d_3\text{-}2^{Me}}$ for the isotopomers $D_3N–BH_3$ and $D_3N–BH_3$ (Supporting Information, Scheme S1 'scramble'), respectively, were also accounted for. In fact, for $D_3N–BH_3$ the scrambling pathway (Tables 1 and S4) provides a smaller computed isotope effect ($K^H_1k^H_2/K^D_1k^D_2$ = 5.3), which will therefore be kinetically preferred, and is in excellent agreement with experiment. In comparison, the 'scrambling' route exhibits a higher normal isotope effect for isotopomer $H_3N–BD_3$ ($K^H_1k^H_2/K^D_1k^D_2$ = 1.7) than the 'non-scrambling' route, also in agreement with experiment.

Catalyst **1** exhibits considerably different KIEs with deuterated substrates than catalyst **2**. While a KIE $k^{\mathrm{H}}_{\mathrm{obs}\mathbf{1}}/k^{\mathrm{D}}_{\mathrm{obs}\mathbf{1}}$ = 1.8 was found for $D_3B–NH_3$, with *N*-deuterated substrates $H_3B–ND_3$ and $D_3B–ND_3$ a shift to zero order dependence of the rate law on substrate was observed, indicating a change in the turn-over limiting step. Also, the spectroscopic characterization of the resulting polyaminoborane indicated some cross-linking for catalyst **2**, which was not observed for **1**. Based on these results, complexes **1** and **2** seem to catalyze AB dehydrocoupling via different mechanisms, and not as active intermediates within the same catalytic cycle, as was previously proposed. However, at the present stage we cannot offer a detailed mechanism for AB dehydrocoupling with catalyst **1** which will be subject to further studies.

CONCLUSIONS

In conclusion, the present paper offers a new mechanistic proposal for the rapid ammonia-borane dehydrocoupling with bifunctional Ru amine catalyst **2**, substantiated by kinetics, aminoborane trapping experiments, stoichiometric reactions with model substrates, and DFT computations. Strong support for the deydrogenation cycle comes from a good agreement of the experimental and computed KIEs. The rapid dehydrogenation rates are attributed to the outer-sphere nature of the mechanism which is associated with low energetic contributions for rearrangement of the first coordination sphere around the metal and to the cooperative behaviour of the PNP ligand. The proposed mechanism with catalytic release of aminoborane upon dehydrogenation of AB and subsequent metal catalyzed B–N coupling to (mainly) polyaminoboranes relies on initial N–H activation as entry to both sub-cycles. This pathway is different to the proposed mechanisms with other catalysts:

1. polyaminoborane formation by initial B–H activation, dehydrogenation, and metal centered B–N coupling without aminoborane release (iridium catalysts),[13,14b]

2. release of catalytically dehydrogenated aminoborane and subsequent uncatalyzed aminoborane oligomerization resulting in formation of borazine and polyborazylene (nickel and Shvo's catalysts).[14b,29]

Low steady-state concentrations of aminoborane are indicated by the initial absence of trapping products and typical, cyclic products from aminoborane oligomerization, which is explained by a catalytic aminoborane enchainment reaction also relying on metal-ligand cooperativity. Therefore, catalyst **2** is considered *bifunctional* in the literal and a figurative sense: (a) two catalyst functional groups are involved in the turnover limiting steps and (b) both dehydrogenation and B-N-coupling are catalyzed. As an interesting consequence of this two stage mechanism, the employment of two separate catalysts, one for dehydrogenation and one for B–N coupling or even for polyaminoborane isomerization in a subsequent treatment, could be a new approach for the synthesis of B–N polymers with well-defined microstructure.

The proposed mechanistic model presented in this paper is highly simplified and does not account quantitatively for some observations, such as polyaminoborane cross-linking, polyborazylene side-product formation, or the mechanistic pathway for our original catalyst **1**. However, it provides an excellent basis for further catalyst design and an important prerequisite to control the microstructure of BN-polymers, which is currently a highly unexplored field.

EXPERIMENTAL SECTION

Materials and Methods. All experiments were carried out under an atmosphere of argon using Schlenk and glove-box techniques. Benzene and THF were dried over Na/benzophenone, distilled under argon and deoxygenated prior to use. Pentane was dried and deoxygenized by passing through columns packed with activated alumina and Q5, respectively. Deuterated solvents were dried by distillation from Na/K alloy (C_6D_6 and d_8-THF), and deoxygenated by three freeze-pump-thaw cycles. KO^{t}Bu was

purchased from VWR and sublimed prior to use. **1** was synthesized as reported earlier and **2** was prepared in situ from the reaction of **1** with H_2 and used as catalyst as a freshly prepared stock solution.[26b] For NMR exchange measurements **2** was prepared in a *J-Young* NMR tube and the latter was subsequently evacuated and backfilled with Argon. AB was purchased from Sigma-Aldrich and sublimed prior to use. Partially and fully deuterated AB were prepared from deuterated starting materials as reported in the literature and were sublimed prior to use.[8j]

Analytical Methods. IR spectra were recorded on a Varian FT/IR-670 spectrometer. NMR spectra were recorded on a Bruker Avance III 400 NMR spectrometer and a JEOL Lambda 400 NMR spectrometer and were calibrated to the residual proton resonance and the natural abundance ^{13}C resonance of the solvent (C_6D_6, δ_H = 7.16 and δ_C = 128.06 ppm; d_8-THF, δ_H = 1.72 and 3.57 ppm, δ_C = 25.3 and 67.4 ppm). ^{31}P NMR chemical shifts are reported relative to external phosphoric acid (δ 0.0 ppm). ^{11}B NMR chemical shifts are reported relative to external BF_3 etherate. Signal multiplicities are abbreviated as: s (singlet), d (doublet), t (triplet), q (quartet), m (multiplet), br (broad). ^1H 2D EXSY NMR spectra were obtained at 300 K in d_8-THF using the Bruker pulse sequence noesyph with D1 set to 2s.

Solid State NMR experiments were conducted at a magnetic field of 11.7 T on a Bruker Avance III-500 spectrometer equipped with a 2.5 mm double resonance MAS probe at ^1H frequency of 500.13 MHz. Saturation combs were used before all repetition delays. The ^1H resonance of 1% tetramethylsilane in $CDCl_3$ served as an external secondary reference for the ^{11}B resonance of $BF_3{\cdot}Et_2O$ in $CDCl_3$ using the Ξ values for ^{11}B as reported by IUPAC.[48]

The ^{11}B MQMAS was performed using a triple-quantum filtered three-pulse sequence with a z-filter and ^1H continuous-wave decoupling[49] implemented with a 24-step nested phase cycle. The repetition delay was set to 0.8 s and acquired 360 transients/FID at a sample spinning frequency ν_r of 25 kHz. The second-order quadrupolar effect (SOQE) parameters and the isotropic chemical shift values were determined by moment analysis[50] and fitting from projections taken from the sheared ^{11}B MQMAS spectrum.

Stoichiometric Experiments. *Synthesis of $H_3N–BEt_3$:* NH_3(g) (15 mL) is dried by condensation into a flask with sodium at –78 °C and subsequently condensed trap-to-trap to a solution of BEt_3 in THF (20 mL, 20 mmol BEt_3). After warming to room temperature and evaporation of NH_3 the solvent is removed i. vac. until a colorless oil remains. Further removal of the solvent at elevated temperatures i. vac. leads to product decomposition. Therefore, the crude product, H_3N-BEt_3 • 0.5 THF, was used as obtained: NMR (C_6D_6, r.t., [ppm]) ^{1}H NMR (399.8 MHz): δ 3.44 (2H, m, CH_2^{THF}), 1.96 (3H, br, NH_3), 1.50 (2H, m, CH_2^{THF}), 0.80 (9H, t, $^3J_{HH}$ = 7.9 Hz, CH_3), 0.19 (6H, q, $^3J_{HH}$ = 7.9 Hz, CH_2). ^{11}B NMR (128.3 MHz): δ –5.3. NMR. (d_8-THF, r.t., [ppm]) ^{1}H NMR (399.8 MHz): δ 3.61 (2H, m, CH_2^{THF}), 3.52 (3H, br, NH_3), 1.77 (2H, m, CH_2^{THF}), 0.74 (9H, t, $^3J_{HH}$ = 7.8 Hz, CH_3), 0.15 (6H, q, $^3J_{HH}$ = 7.8 Hz, CH_2). ^{11}B NMR (128.3 MHz): δ -5.9. ^{13}C {^{1}H} NMR (100.6 MHz): δ 68.2 (s, CH_2^{THF}), 26.4 (s, CH_2^{THF}), 15.4 (br, CH_2), 10.2 (s, CH_3). Assignments were confirmed by ^{13}C {^{1}H} DEPT NMR.

*Reaction of **2** with $Et_3B–NH_3$.* **2** (14.7 μmol) is mixed with BEt_3NH_3 · 0.5 THF (22.0 μmol, 1.5 equiv) in dry d_8-THF in a *J-Young* NMR tube. Small amounts of **4** are observed in the ^{1}H, ^{31}P and ^{11}B NMR spectra. Selected NMR data of **4** (d_8-THF, r.t., [ppm]): ^{1}H NMR (399.8 MHz): δ 6.50 (1H, s br, NH), 3.19 (2H, m, Ru-NH_2-B), 1.40 (d, $^2J_{HP}$ = 7.4 Hz, 9H, $P(CH_3)_3$), 0.66 (9H, t, $^3J_{HH}$ = 7.6 Hz, $CH_3^{BEt3NH2}$), 0.08 (6H, q, $^3J_{HH}$ = 7.6 Hz, $CH_2^{BEt3NH2}$), –18.44 (1 H, q, $^2J_{HP}$ = 24.1 Hz, Ru-H). ^{31}P{^{1}H} NMR (161.83 MHz): δ 62.1 (d, $^2J_{PP}$ =29.5 Hz, P^{i}Pr$_2$), 10.3 (t, $^2J_{PP}$ =29.5 Hz, $P(CH_3)_3$). ^{11}B NMR (128.3 MHz): δ –3.1 (s). With mixing times of τ_m = 500 ms and 1000 ms cross peaks between BEt_3NH_3 and the hydride adjacent to the N–H proton of **2** were observed in the ^{1}H 2D EXSY NMR spectra (Supporting Information Figure S5).

*Reaction of **3** with $Et_3B–NH_3$.* **3** (10.0 mg, 20.1 μmol) is dissolved in dry d_8-THF in a *J-Young* NMR tube with BEt_3NH_3 · 0.5 THF (4.5 mg, 29.8 μmol, 1.5 equiv). With mixing times of τ_m = 500 ms and 1000 ms no exchange peaks between NH_3BEt_3 and the hydrides of **3** were observed by *^{1}H 2D EXSY NMR* spectra.

*Reaction of **2** with $Et_3B–NH_3$ and $H_3B–NMe_3$.* $Et_3B–NH_3 \cdot 0.5$ THF (8.2 mg, 54.5 μmol) and $H_3B–NMe_3$ (3.8 mg, 52.1 μmol) are added to a solution of **2** (0.46 μmol; 0.9 mol%) in 0.4 mL d_8-THF in a *J-Young*-NMR tube. Over the course of 24 h no coupling reaction was observed at room temperature by ^{11}B and ^{1}H NMR spectroscopy.

Kinetic Experiments. *Catalytic Protocols*: In a typical experiment, $H_3B–NH_3$ (46.3 mg; 1.5 mmol) is dissolved in THF in a Schlenk tube connected to a water-filled graduated cylinder (eudiometer). A solution of the corresponding catalyst in THF is quickly added via syringe. The volume of collected hydrogen gas is recorded in adequate time spans.

*Aminoborane Trapping with **1**.* Cyclohexene (1.5 mL, 14.8 mmol, 21 eq) is added to a solution of $H_3N–BH_3$ (22.0 mg, 0.7 mmol, 0.2 M) in THF (1.5 mL). After addition of **1** (0.7 mol%), the reaction mixture is stirred for 10 min at r.t. in a vented vial. The ^{11}B NMR spectrum of an aliquot of the white suspension shows a broad peak for polyborazylene as the only product. After 24 h a dublet for borazine and a broad singlet at 48.4 ppm appear.

*Aminoborane Trapping with **2**.* To a suspension of $H_3N–BH_3$ (22.0 mg, 0.7 mmol, 0.2 M) in cyclohexene (1.5 mL, 14.8 mmol, 21 equiv) a solution of **2** (2.5 mg, 5.0 μmol, 0.7 mol%) in THF (1.5 mL) is added. The reaction mixture is stirred for 10 min at r.t. in a vented vial. The ^{11}B NMR spectrum of an aliquot of the white suspension shows a dublet for borazine ($\delta = 31.1$ ppm), polyborazylene ($\delta = 26.0$ ppm) and **A** ($\delta = –5.0$ ppm, –11.0 ppm, –23.0 ppm). After 24 h a broad singlet at 48.4 ppm appears.

*Aminoborane Trapping with **3**.* Cyclohexene (0.8 mL, 7.9 mmol, 21 equiv) is added to a solution of H_3N-BH_3 (11.5 mg, 0.37 mmol, 0.1 M) in THF (3 mL). After addition of **3** (0.1 mol%) the reaction mixture is stirred for 3.5 h at r.t. in a vented vial. The ^{11}B NMR spectrum of an aliquot of the slightly turbit reaction solution shows aside from starting material ($\delta = –21.6$ ppm) signals for borazine ($\delta = 31.1$ ppm), polyborazylene ($\delta = 26.0$ ppm), **A** ($\delta = –5.0$ ppm, –11.0 ppm, –23.0 ppm) and a broad

peak at 48.4 ppm, indicating the trapping of free aminoborane by hydroboration of cyclohexene (Supporting Information).

Characterization of the dehydrocoupling product ***C***: A solution of **1** (0.75 mg; 1.6 μmol) in 1 mL THF is pressurized with H_2 and catalyst **2** is formed *in situ*. 0.5 mL of this stock solution (0.02 mol%) is added via syringe to a vigorously stirred solution of H_3B-NH_3 (93.0 mg; 3.0 mmol) in 0.7 mL THF. After evolution of 1 equiv H_2 at rt the suspension is filtered. The white residue is washed with THF (3 x 5mL) and pentane (3 x 5 mL) and dried *i. vac*. Yield: 85.0 mg (2.9 mmol; 98%). Anal. Calcd. for H_4BN (28.85): H, 13.98; N, 48.55. Found: H, 13.31; N, 44.73; C, 2.89 from residual solvent. IR (ATR, cm^{-1}): 3300 (s, N–H_{asym}), 3247 (s, N–H_{sym}), 2382-2311 (B–H), 1558 (s) (Figure S6).

Characterization of the dehydrocoupling product ***D***: A solution of **3** (0.75 μmol; 0.05 mol%) in 0.3 mL THF is added via syringe to a vigorously stirred solution of H_3B–NH_3 (46.0 mg; 1.5 mmol; 2.5 M) in 0.3 mL THF. After evolution of 1 equiv H_2 at r.t., the suspension is filtered. The white residue is washed with THF (3 x 5mL) and pentane (3 x 5 mL) and dried *i. vac*. Yield: 39.0 mg (1.223 mmol; 82 %). Anal. Calcd. for H_4BN (28.85): H, 13.98; N, 48.55. Found: H, 13.39; N, 44.46; C, 3.99 (from residual solvent). IR (ATR, cm^{-1}): 3298 (s, N–H_{asym}), 3248 (s, N–H_{sym}), 2386-2314 (B–H), 1557 (s) (Figure S7).

DFT calculations. All calculations were performed with GAUSSIAN-03 Rev. C.02 using the density functional/Hartree-Fock hybrid model Becke3LYP and the split valence double-ζ (DZ) basis set 6-31+G**.[51,52,53] The Ru atoms were described with a Stuttgart-RSC-ECP with a DZ description of the valence electrons.[54] Geometry optimizations were run without symmetry or internal coordinate constraints. The optimized structures were verified as being true minima (NImag=0) or transition states (NImag=1) by analysis of negative eigenvalues in vibrational frequency calculations. Thermal corrections were carried out at standard conditions (T = 298.15 K, and P = 1 atmosphere). The theoretical values of KIEs have been determined by substituting H to D in the optimized structures and applying the force constants of the frequency calculation to obtain the changed thermodynamical values

(especially the Gibbs free energy). No further optimization has been applied for the deuteriated species. The KIE is then calculated from the ΔG barrier heights of the relevant non-deuterated and deuterated transition states via equation 4.

Acknowledgement. This contribution is dedicated to the memory of Prof. Dr. Keith Fagnou. The authors thank the DFG (grants SCHN 950/2-1 and SCHN 950/4-1) and the Fonds der chemischen Industrie, for funding and the Elitenetzwerk Bayern for a graduate fellowship (A.F.). M.D. expresses his gratitude to the Leibniz-Computing Center for the infrastructure provided for the DFT calculations.

Supporting Information Available: Kinetic, spectroscopic, and computational details: this material is free of charge via the internet at http://pubs.acs.org/.

REFERENCES

(1) Reviews: (a) Stephens, F. H.; Pons, V.; Baker, R. T. *DaltonTrans.* **2007**, 2613. (b) Hamilton, C. W.; Baker, R. T.; Staubitz, A.; Manners, I. *Chem. Soc. Rev.* **2009**, *38*, 279. (c) Smythe, N. C.; Gordon, J. C. *Eur. J. Inorg. Chem.* **2010**, 509. (d) Staubitz, A.; Robertson, A. P. M.; Manners, I. *Chem. Rev.* **2010**, *110*, 4079.

(2) (a) Davis, B. L.; Dixon, D. A.; Garner, E. B.; Gordon, J. C.; Matus, M. H.; Scott, B.; Stephens, F. H. *Angew. Chem.* **2009**, *121*, 6944; *Angew. Chem. Int. Ed.* **2009**, *48*, 6812. (b) Sutton, A. D.; Burrell, A. K.; Dixon, D. A.; Garner III., E. B.; Gordon, J. C.; Nakagawa, T.; Ott, K. C.; Robinson, P.; Vasiliu, M. *Science* **2011**, *331*, 1426. (c) Reller, C.; Mertens, F. O. R. L. *Angew. Chem.* **2012**, *124*, 11901; *Angew. Chem. Int. Ed.* **2012**, *51*, 11731.

(3) Reviews: (a) Clark, T. J.; Lee, K.; Manners, I. *Chem. Eur. J.* **2006**, *12*, 8634. (b) Staubitz, A.; Robertson, A. P. M.; Sloan, M. E.; Manners, I. *Chem. Rev.* **2010**, *110*, 4023. (c) Whittell, G. R.; Manners, I. *Angew. Chem.* **2011**, *123*, 10470; *Angew. Chem. Int. Ed.* **2011**, *50*, 10288.

(4) Bluhm, M. E. ; Bradley, M. G.; Butterick III, R.; Kusari, U.; Sneddon, L. G. *J. Am. Chem. Soc.* **2006**, *128*, 7748.

(5) Stephens, F. H.; Baker, R. T.; Matus, M. H.; Grant, D. J.; Dixon, D. A. *Angew. Chem.* **2007**, *119*, 760; *Angew. Chem. Int. Ed.* **2007**, *46*, 746.

(6) Himmelberger, D. W.; Yoon, C. W.; Bluhm, M. E.; Carroll, P. J.; Sneddon, L. G. *J. Am. Chem. Soc.* **2009**, *131*, 14101.

(7) (a) Spielmann, J.; Bolte, M.; Harder, S. *Chem. Commun.* **2009**, 6934. (b) Liptrot, D. J.; Hill, M. S.; Mahon, M. F.; MacDougall, D. J. *Chem. Eur. J.* **2010**, *16*, 8508.

(8) Miller, A. J. M.; Bercaw, J. E. *Chem. Commun.* **2010**, *46*, 1709.

(9) (a) Clark, T. J.; Russell, C. A.; Manners, I. *J. Am. Chem. Soc.* **2006**, *128*, 9582. (b) Pun, D.; Lobkovsky, E.; Chirik, P. J. *Chem. Commun* **2007**, 3297. (c) Sloan, M. E.; Staubitz A.; Clark, T. J.; Russell, C. A.; Lloyd-Jones, G. C.; Manners, I. *J. Am. Chem. Soc.* **2010**, *132*, 3831. (d) Miyazaki, T.; Tanabe, Y.; Yuki, M.; Miyake, Y.; Nishibayashi, Y. *Organometallics* **2011**, *30*, 2394. (e) Beweries, T.; Thomas, J.; Klahn, M.; Heller, D.; Schulz, A.; Rosenthal, U. *ChemCatChem* **2011**, *3*, 1865.

(10) (a) Jiang, Y.; Berke, H. *Chem Commun.* **2007**, 3571. (b) Jiang, Y.; Blacque, O.; Fox, T.; Frech, C. M.; Berke, H. *Organometallics* **2009**, *28*, 5493. (c) Kawano, Y.; Uruichi, M.; Shimoi, M.; Taki, S.; Kawaguchi, T.; Kakizawa, T.; Ogino, H. *J. Am. Chem. Soc.* **2009**, *131*, 14946. (d) Vance, J. R.; Robertson, A. P. M.; Lee, K.; Manners, I. *Chem Eur. J.* **2011**, *17*, 4099.

(11) Ruthenium: (a) Mal, S. S.; Stephens, F. H.; Baker, R. T. *Chem. Commun.* **2011**, *47*, 2922. (b) Wright, W. R. H.; Berkeley, E. R.; Alden, L. R.; Baker, R. T.; Sneddon, L. G. *Chem. Commun.* **2011**, *47*, 3177. (c) Ledger, A. E. W.; Ellul, C. E.; Mahon, M. F.; Williams, J. M. J.; Whittlesey, M. K. *Chem. Eur. J.* **2011**, *17*, 8704.

(12) Rhodium: (a) Jaska, C. A.; Temple, K.; Lough, A. J.; Manners, I. *Chem. Commun.* **2001**, 962. (b) Jaska, C. A.; Temple, K.; Lough, A. J.; Manners, I. *J. Am. Chem. Soc.* **2003**, *125*, 9424. (c) Jaska, C. A.; Manners, I. *J. Am. Chem. Soc.* **2004**, *126*, 1334. (d) Jaska, C. A.; Manners, I. *J. Am. Chem. Soc.* **2004**, *126*, 9776. (e) Chen, Y.; Fulton, J. L.; Linehan, J. C.; Autrey, T. *J. Am. Chem. Soc.* **2005**, *127*, 3254. (f) Fulton, J. F.; Linehan, J. C.; Autrey, T.; Balasubramanian, M.; Chen, Y.; Szymczak, N. K. *J. Am. Chem. Soc.* **2007**, *129*, 11936. (g) Douglas, T. M.; Chaplin, A. B.; Weller, A. S. *J. Am. Chem. Soc.* **2008**, *130*, 14432. (h) Sloan, M. E.; Clark, T. J.; Manners, I. *Inorg. Chem.* **2009**, *48*, 2429. (i) Rousseau, R.; Schenter, G. K.; Fulton, J. L.; Linehan, J. C.; Linehan, M. K.; Engelhard, M. K.; Autrey, T. *J. Am. Chem. Soc.* **2009**, *131*, 10516. (j) Dallanegra, R.; Robertson, A. P. M.; Chaplin, A. B.; Manners, I.; Weller, A. S. *Chem. Commun.* **2011**, *47*, 3763.

(13) Iridium: (a) M. C. Denney, V. Pons, T. J. Hebden, D. M. Heinekey, K. I. Goldberg, *J. Am. Chem. Soc.* **2006**, *128*, 12048. (b) B. L. Dietrich, K. I. Goldberg, D. M. Heinekey, T. Autrey, J. C. Linehan, *Inorg. Chem.* **2008**, *47*, 8583. (c) A. Staubitz, A. Presa Soto, I. Manners, *Angew. Chem.* **2008**, *120*, 6308; *Angew. Chem. Int. Ed.* **2008**, *47*, 6212. (d) A. Staubitz, M. E. Sloan, A. Robertson, A. Friedrich, S. Schneider, P. J. Gates, J. Schmedt auf der Günne, I. Manners, *J. Am. Chem. Soc.* **2010**, *132*, 13332. (e) Johnson, H. C.; Robertson, A. P. M.; Chaplin, A. B.; Sewell, L. J.; Thompson, A. L.; Haddow, M. F.; Manners, I.; Weller, A. S. *J. Am. Chem. Soc.* **2011**, *133*, 11076.

(14) Nickel: (a) Keaton, R. J.; Blacquiere, J. M.; Baker, R. T. *J. Am. Chem. Soc.* **2007**, *129*, 1844. (b) Pons, V.; Baker, R. T.; Szymczak, N. K.; Heldebrant, D. J.; Linehan, J. C.; Matus, M. H.; Grant, D. J.; Dixon, D. A. *Chem. Commun.* **2008**, 6597. (c) Vogt, M.; de Bruin, B.; Berke, H.; Trincado, M.; Grützmacher, H. *Chem. Sci.* **2011**, *2*, 723.

(15) Alcaraz, G.; Sabo-Etienne, S. *Angew. Chem.* **2010**, *122*, 7326; *Angew. Chem. Int. Ed.* **2010**, *49*, 7170.

(16) (a) Douglas, T. M.; Chaplin, A. B.; Weller, A. S. *J. Am. Chem. Soc.* **2008**, *130*, 14432. (b) Dallanegra, R.; Chaplin, A. B.; Weller, A. S. *Angew. Chem.* **2009**, *121*, 7007; *Angew. Chem. Int. Ed.* **2009**, *48*, 6875. (c) Dallanegra, R.; Chaplin, A. B.; Tsim, J.; Weller, A. S. *Chem Commun.* **2010**, *46*, 3092. (d) Chaplin, A. B.; Weller, A. S. *Inorg. Chem.* **2010**, *49*, 1111. (e) Alcaraz, G.; Vendier, L.; Clot, E.; Sabo-Etienne, S. *Angew. Chem.* **2010**, *122*, 930; *Angew. Chem. Int. Ed.* **2010**, *49*, 918. (f) Tang, C. Y.; Thompson, A. L.; Aldridge, S. *Angew. Chem.* **2010**, *122*, 933; *Angew. Chem. Int. Ed.* **2010**, *49*, 921. (g) Tang, C. Y.; Thompson, A. L.; Aldridge, S. *J. Am. Chem. Soc.* **2010**, *132*, 10578. (h) Johnson, H. C.; Robertson, A. P. M.; Chaplin, A. B.; Sewell, L. J.; Thompson, A. L.; Haddow, M. F.; Manners, I.; Weller, A. S. *J. Am. Chem. Soc.* **2011**, *133*, 11076.

(17) Chaplin, A. B.; Weller, A. S. *Angew. Chem.* **2010**, *122*, 473; *Angew. Chem. Int. Ed.* **2010**, *49*, 581.

(18) (a) Douglas, T. M.; Chaplin, A. B.; Weller, A. S.; Yang, X.; Hall, M. B. *J. Am. Chem. Soc.* **2009**, *131*, 15440. (b) Stephens, C. J.; Dallanegra, R.; Chaplin, A. B.; Weller, A. S.; Macgregor, S. A.; Ward, B.; McKay, D.; Alcaraz, G.; Sabo-Etienne, S. *Chem. Eur. J.* **2011**, *17*, 3011. (c) Sewell, L. J.; Lloyd-Jones, G. C.; Weller, A. S. *J. Am. Chem. Soc.* **2012**, *134*, 3598.

(19) B. L. Dietrich, K. I. Goldberg, D. M. Heinekey, T. Autrey, J. C. Linehan, *Inorg. Chem.* **2008**, *47*, 8583.

(20) Chen, X.; Zhao, J.-C.; Shore, S. G. *J. Am. Chem. Soc.* **2010**, *132*, 10658.

(21) Paul, A.; Musgrave C. B. *Angew. Chem.* **2007**, *119*, 8301; *Angew. Chem. Int. Ed.* **2007**, *46*, 8153.

(22) (a) Yang, X.; Hall, M. B. *J. Am. Chem. Soc.* **2008**, *130*, 1798. (b) Yang, X.; Hall, M. B. *J. Organomet. Chem.* **2009**, *694*, 2831.

(23) (a) Kwon, C. T.; McGee, H. A. *Inorg. Chem.* **1970**, *9*, 2458. (b) Wang, J. S.; Geneangel, R. A. *Inorg. Chim. Acta* **1988**, *148*, 185.

(24) Zimmerman, P. M.; Paul, A.; Zhang, Z.; Musgrave, C. B. *Inorg. Chem.* **2009**, *48*, 1069.

(25) Shaw, W. J.; Linehan, J. C.; Szymczak, N. K.; Heldebrant, D. J.; Yonker, C.; Camaioni, D. M.; Baker, R. T.; Autrey, T. *Angew. Chem.* **2008**, *120*, 7603; *Angew. Chem.* **2008**, *47*, 7493.

(26) (a) Blaquiere, N.; Diallo-Garcia, S.; Gorelsky, S. I.; Black, D. A.; Fagnou, K. *J. Am. Chem. Soc.* **2008**, *130*, 14034. (b) Käß, M.; Friedrich, A.; Drees, M.; Schneider, S. *Angew. Chem.* **2009**, *121*, 922; *Angew. Chem. Int. Ed.* **2009**, *48*, 905

(27) Chapman, A. M.; Haddow, M. F.; Wass, D. F. *J. Am. Chem. Soc.* **2011**, *133*, 8826.

(28) Baker, R. T.; Gordon, J. C.; Hamilton, C. W.; Henson, N. J.; Lin, P.-H.; Maguire, S.; Murugesu, M.; Scott, B. L.; Smythe, N. C. *J. Am. Chem. Soc.* **2012**, *134*, 5598.

(29) (a) Conley, B. L. ; Williams, T. J. *Chem. Commun.* **2010**, *46*, 4815. (b) Lu, Z.; Conley, B. L.; Williams, T. J. *Organometallics* **2012**, *31*, 6705.

(30) Conley, B. L.; Guess, D.; Williams, T. J. *J. Am. Chem. Soc.* **2011**, *133*, 14212.

(31) Friedrich, A.; Drees, M.; Schneider, S. *Chem. Eur. J.* **2009**, *15*, 10339.

(32) Friedrich, A.; Drees, M.; Käß, M.; Herdtweck, E.; Schneider, S. *Inorg. Chem.* **2010**, *49*, 5482.

(33) Friedrich, A; Drees, M.; Schmedt auf der Günne, J.; Schneider, S. *J. Am. Chem. Soc.* **2009**, *131*, 17552.

(34) Swinnen, S.; Nguyen, V. S.; Nguyen, M. T. *Chem Phys. Lett.* **2011**, *513*, 195.

(35) The concentration of AB was derived by the idealized stoichiometry for the reaction in Scheme 3, which should be a good approximation for low conversions. The small amount of H_2 formation from borazine production has been neglected in this expression.

(36) This value is slightly smaller than our original estimate (2.1) where the full plot over 2 half-lifes was used and the initiation period was not accounted for.[26b]

(37) The slight deviation possibly points towards an induction period. As one of the reviewers pointed out, it could also be an artefact from eudiometry that arises from AB conversion without H_2 release, as proposed for the initiation period of chain growth in base catalyzed AB dehydrocoupling.[38] However, in contrast to this mechanism trapping experiments with cyclohexene indicate the release of free aminoborane with catalyst **3** (c.f. section 2.2).

(38) Ewing, W. C.; Marchione, A.; Himmelberger, D. W.; Carroll, P. J.; Sneddon, L. G. *J. Am. Chem. Soc.* **2011**, *133*, 17093.

(39) Shresta, R. P.; Diyabalanage, H. V. K.; Semelsberger, T. A.; Ott, K. C.; Burrell, A. K. *Int. J. Hydrogen Energy* **2009**, *34*, 2616.

(40) The absence of AB in the sample of **B** is evidenced by the ^{11}B MQMAS line-shape.

(41) (a) Kim, D.-P.; Moon, K.-T.; Kho, J.-G.; Economy, J.; Gervais, C.; Babonneau, F. *Polym. Adv. Technol.* **1999**, *10*, 702. (b) Gervais, C.; Babonnaeu, F. J. *Organomet. Chem.* **2002,** *657,* 75. (c) Baumann, J.; Baitalow, J.; Wolf, G. *Thermochim Acta* **2005**, *430*, 9.

(42) Nöth, H.; Vahrenkamp, H. *Chem. Ber.* **1966**, *99*, 1049.

(43) Sana, M.; Leroy, G. *Int. J. Quantum Chem.* **1993**, *48*, 89.

(44) Avadhut, Y. S.; Schneider, D.; Schmedt auf der Günne, J. *J. Magn. Reson.* **2009**, *201*, 1.

(45) A. P. M. Robertson, E. M. Leitao, I. Manners, *J. Am. Chem. Soc.* **2011**, *133*, 19322.

(46) The concentration of AB was not directly measured but calculated from H2 release. Hence, the consumption of AB by aminoborane insertion into an N–H bond is ignored in this model. However, the resulting linear diborazane (or higher borazanes at a later stage) should exhibit comparable barriers for terminal dehydrogenation. Note that both the initial rate method and first order kinetic plots gave identical experimental rate constants.

(47) (a) Landis, C. R.; Hilfenhaus, P.; Feldgus, S. *J. Am. Chem. Soc.* **1999**, *121*, 8741. (b) Zimmer-De Iuliis, M.; Morris, R. H. *J. Am. Chem. Soc.* **2009**, *131*, 11263.

(48) Harris, R. K.; Becker, E. D.; Cabral de Menezes, S. M.; Granger, P.; Hoffman, R. E.; Zilm, K. W. *Pure Appl. Chem.* **2008**, *80*, 59.

(49) Fernandez, C.; Amoureux, J. P. *Solid State Nucl. Magn. Reson.* **1996**, *5*, 315.

(50) (a) Amoureux, J.-P.; Fernandez, C.; Steuernagel, S. *J. Magn. Reson. A* **1996**, *123*, 116. (b) Herreros, B.; Metz, A. W.; Harbison, G. S. *Solid State Nucl. Magn. Reson.* **2000**, *16*, 141.

(51) Gaussian 03, Revision C.02, Frisch, M. J.; Trucks, G. W.; Schlegel, H. B.; Scuseria, G. E.; Robb, M. A.; Cheeseman, J. R.; Montgomery, Jr., J. A.; Vreven, T.; Kudin, K. N.; Burant, J. C.; Millam, J. M.; Iyengar, S. S.; Tomasi, J.; Barone, V.; Mennucci, B.; Cossi, M.; Scalmani, G.; Rega, N.; Petersson, G. A.; Nakatsuji, H.; Hada, M.; Ehara, M.; Toyota, K.; Fukuda, R.; Hasegawa, J.; Ishida, M.; Nakajima, T.; Honda, Y.; Kitao, O.; Nakai, H.; Klene, M.; Li, X.; Knox, J. E.; Hratchian, H. P.; Cross, J. B.; Bakken, V.; Adamo, C.; Jaramillo, J.; Gomperts, R.; Stratmann, R. E.; Yazyev, O.; Austin, A. J.; Cammi, R.; Pomelli, C.; Ochterski, J. W.; Ayala, P. Y.; Morokuma, K.; Voth, G. A.; Salvador, P.; Dannenberg, J. J.; Zakrzewski, V. G.; Dapprich, S.; Daniels, A. D.; Strain, M. C.; Farkas, O.; Malick, D. K.; Rabuck, A. D.; Raghavachari, K.; Foresman, J. B.; Ortiz, J. V.; Cui, Q.; Baboul, A. G.; Clifford, S.; Cioslowski, J.; Stefanov, B. B.; Liu, G.; Liashenko, A.; Piskorz, P.; Komaromi, I.; Martin, R. L.; Fox, D. J.; Keith, T.;

Al-Laham, M. A.; Peng, C. Y.; Nanayakkara, A.; Challacombe, M.; Gill, P. M. W.; Johnson, B.; Chen, W.; Wong, M. W.; Gonzalez, C.; Pople, J. A.; Gaussian, Inc., Wallingford CT, 2004.

(52) (a) Vosko, S. H.; Wilk, L.; Nusair, M. Can. J. Phys. 1980, 58, 1200-1211. (b) Lee, C.; Yang, W.; Parr, R. G. *Phys. Rev. B.* **1988**, 37, 785-789. (c) Becke, A. D. *J. Chem. Phys.* **1993**, *98*, 5648-5652.

(53) (a) Hehre, W. J.; Ditchfield, R.; Pople, J. A. *J. Chem. Phys.* **1972**, *56*, 2257-2261. (b) Francl, M.M.; Pietro, W.J.; Hehre, W.J.; Binkley, J.S.; Gordon, M.S.; DeFrees D.J. and Pople, J.A. *J. Chem. Phys.* **1982**, *77*, 3654-3665.

(54) Dolg, M.; Stoll, H.; Preuss, H.; Pitzer, R.M. *J. Phys. Chem.* **1993**, *97*, 5852.

TOC Figure.